

1 **Phospholipid peroxidation fuels ExoU phospholipase-dependent cell necrosis**
2 **and supports *Pseudomonas aeruginosa*-driven pathology**

3 Salimata Bagayoko¹, Stephen Leon Icaza^{1§}, Miriam Pinilla^{1§}, Audrey Hessel^{1§}, Karin
4 Santoni¹, Pierre-Jean Bordignon¹, Flavie Moreau^{1,2}, Elif Eren¹, Aurélien Boyancé¹,
5 Emmanuelle Naser^{1,3}, Lise Lefèvre⁴, Céline Berrone^{1,2}, Nino Iakobachvili⁸, Arnaud
6 Metais¹, Yoann Rombouts¹, Agnès Coste⁴, Ina Attrée⁵, Dara W. Frank⁶, Hans
7 Clevers⁷, Peter J. Peters⁸, Céline Cougoule¹, Rémi Planès^{1#} & Etienne Meunier^{1#}

8

9 ¹ Institute of Pharmacology and Structural Biology (IPBS), University of Toulouse,
10 CNRS, Toulouse; France

11 ² Level 3 Biosafety Animal Core facility, Anexplo platform, Institute of Pharmacology
12 and Structural Biology (IPBS), University of Toulouse, CNRS, Toulouse; France

13 ³ Cytometry & Imaging Core facility, Institute of Pharmacology and Structural Biology
14 (IPBS), University of Toulouse, CNRS, Toulouse; France

15 ⁴ RESTORE institute, University of Toulouse, CNRS, Toulouse; France

16 ⁵ Univ. Grenoble Alpes, CNRS, CEA, IBS, Bacterial Pathogenesis and Cellular
17 Responses, F-38000 Grenoble

18 ⁶ Department of Microbiology and Immunology, Medical College of Wisconsin,
19 Milwaukee, WI, 53226; USA

20 ⁷ Oncode Institute, Hubrecht Institute, Royal Netherlands Academy of Arts and
21 Sciences and University Medical Center, Utrecht, Netherlands

22 ⁸ Division of Nanoscopy, Maastricht Multimodal Molecular Imaging Institute,
23 Maastricht University, The Netherlands

24

25 § These authors contributed equally

26 # Address correspondence to: etienne.meunier@ipbs.fr (EM) & remi.planes@ipbs.fr
27 (RP)

28 Lead contact: etienne.meunier@ipbs.fr (EM)

29

30 Present Address: Institute of Pharmacology and Structural Biology (IPBS), 205 Route
31 de Narbonne, CNRS, 31000 Toulouse; France

32

33 **Summary**

34 Regulated cell necrosis supports immune and anti-infectious strategies of the body;
35 however, dysregulation of these processes drives pathological organ damage.
36 *Pseudomonas aeruginosa* expresses a phospholipase, ExoU that triggers
37 pathological host cell necrosis through a poorly characterized pathway. Here, we
38 investigated the molecular and cellular mechanisms of ExoU-mediated necrosis. We
39 show that cellular peroxidised phospholipids enhance ExoU phospholipase activity,
40 which drives necrosis of immune and non-immune cells. Conversely, both the
41 endogenous lipid peroxidation regulator GPX4 and the pharmacological inhibition of
42 lipid peroxidation delay ExoU-dependent cell necrosis and improve bacterial
43 elimination *in vitro* and *in vivo*. Our findings also pertain to the ExoU-related
44 phospholipase from the bacterial pathogen *Burkholderia thailandensis*, suggesting
45 that exploitation of peroxidised phospholipids might be a conserved virulence
46 mechanism among various microbial phospholipases. Overall, our results identify an
47 original lipid peroxidation-based virulence mechanism as a strong contributor of
48 microbial phospholipase-driven pathology.

49

50 Key words: lipid peroxidation, microbial phospholipases, cell necrosis, *Pseudomonas*
51 *aeruginosa*

52

53

54

55

56

57

58

59

60

61

62 Introduction

63 Regulated cell necrosis (RCNs) drives physiological and immune processes, yet
64 dysregulation of this process promotes pathological responses such as organ-failure
65 and sepsis (Bedoui et al., 2020; Galluzzi et al., 2018; Place et al., 2021; Tang et al.,
66 2020). Mechanistically, oxygen-dependent cell death is an evolutionary conserved
67 process that involves the production of reactive oxygen species (ROS), transition
68 metals (e.g. iron) and peroxidised lipid accumulation (Bogacz and Krauth-Siegel,
69 2018; Conrad et al., 2018; Dixon et al., 2012; Jenkins et al., 2020). In addition to cell
70 necrosis, lipid peroxidation broadly involves cellular processes essential to mediate
71 optimal efferocytosis of dead cells, cellular communication resulting from the
72 formation of lipids derived from peroxidised phospholipids (e.g. isoprostanes, platelet
73 activating factor) or the production of bioactive lipids (eicosanoids) from arachidonic
74 acid (Bochkov et al., 2010; Tyurina et al., 2019). In addition, the peroxidation of the
75 mitochondrial phospholipid cardiolipin initiates apoptosis while the accumulation of
76 peroxidised phosphatidyl ethanolamines (PE) promote the cellular necrosis,
77 ferroptosis (Bersuker et al., 2019; Conrad and Pratt, 2019; Doll et al., 2017, 2019;
78 Kagan et al., 2017; Wiernicki et al., 2020; Yang et al., 2016). Specifically, the
79 dysregulation of lipid peroxidation processes is associated with various human
80 pathologies such as cancer chemoresistance, brain and ischemia injuries,
81 neurological alterations, metabolic diseases as well as tuberculosis susceptibility
82 (Amaral et al., 2019; Dar et al., 2018; Li et al., 2020; Meunier and Neyrolles, 2019;
83 Stockwell et al., 2020; Zhu et al., 2019). In this context, the enzymes glutathione
84 peroxidase 4 (GPX4) and ferroptosis-suppressor protein-1 (FSP1) that belongs to the
85 CoQ antioxidant system, detoxify phospholipid hydroperoxide accumulation, hence
86 allowing lipid peroxide amounts to be balanced in cells (Bersuker et al., 2019; Dixon
87 et al., 2012; Doll et al., 2019; Friedmann Angeli et al., 2014; Yang et al., 2016). On
88 the contrary, iron excess, lipoxygenase activity or cytochrome P450 oxidoreductase
89 (CYPOR) all promote phospholipid peroxidation, which can end with ferroptosis
90 induction in the absence of proper regulation (Dixon et al., 2012; Doll et al., 2017;
91 Kagan et al., 2017; Yan1 et al., 2020; Yang et al., 2016; Zou et al., 2020).

92 In this regard, the bacterial pathogen *Pseudomonas aeruginosa* (*P. aeruginosa*)
93 expresses ExoU, an A2 phospholipase from the patatin family, that triggers a
94 necrosis-dependent pathology through a poorly understood pathway (Anderson et

95 al., 2015; Dessen, 2000; Diaz and Hauser, 2010; Gendrin et al., 2012; Howell et al.,
96 2013; Phillips et al., 2003; Rabin and Hauser, 2003; Sato and Frank, 2004; Sitkiewicz
97 et al., 2006; Wilson and Knoll, 2018). In presence of cellular co-factors such as
98 ubiquitin (Anderson et al., 2015) or the trafficking chaperone DNAJC5 (Deruelle et al.,
99 2020), ExoU activity rapidly cleaves at the sn-2 position of host membrane
100 phospholipids, liberating large amounts of arachidonic acid that are then metabolized
101 into eicosanoids by cellular enzymes cyclooxygenases, cytochrome P450 or
102 lipoxygenases (Machado et al., 2011; Pazos et al., 2017; Saliba et al., 2005; Wilson
103 and Knoll, 2018). Importantly, *in vivo*, ExoU expression by *P. aeruginosa* is
104 associated with a robust production of oxidized lipids such the platelet activating
105 factor (PAF) or isoprostanes (da Cunha et al., 2015; Machado et al., 2011). In this
106 context, we explored the possibility that *P. aeruginosa* ExoU mediates a necrosis-
107 dependent host pathology involving lipid peroxidation.

108

109

110

111

112

113

114

115

116

117

118

119

120

121

122

123 ***P. aeruginosa* infection triggers ExoU-dependent alarmin and peroxidised lipid**
124 **production in mice**

125 *P. aeruginosa* ExoU is injected into cells by the Type-3 Secretion System (T3SS)
126 (Gendrin et al., 2012; Rabin and Hauser, 2003), which triggers a fast and violent
127 cellular necrosis. Therefore, we first monitored the profile of ExoU-dependent
128 pathology in mice infected with the clinical isolate pp34 *exoU*⁺ or its isogenic mutant
129 (*exoU*). Similar to previous studies (Howell et al., 2013; Al Moussawi and
130 Kazmierczak, 2014; Phillips et al., 2003; Shaver and Hauser, 2004), intranasal
131 instillation with either *exoU*⁺ or *exoU* strains highlighted a *P. aeruginosa*-induced
132 acute pathology mainly due to ExoU, as mice infected with *exoU* bacteria showed
133 improved survival to infection (**Fig. 1A**). This observation was paralleled with lower
134 bacterial loads of *P. aeruginosa* *exoU* than *exoU*⁺ in the bronchoalveolar lavage
135 fluids (BALFs), the lungs, the blood and the spleen, suggesting that ExoU also
136 promotes bacterial dissemination (**Fig. 1B**). As *P. aeruginosa* triggers NLR4-,
137 NLRP3- and Caspase-11-dependent inflammasome response (Balakrishnan et al.,
138 2018; Bitto et al., 2018; Cohen and Prince, 2013; Eren et al., 2019; Faure et al.,
139 2014; Franchi et al., 2007; Iannitti et al., 2016; Miao et al., 2008; Al Moussawi and
140 Kazmierczak, 2014; Santos et al., 2018; Sutterwala et al., 2007), we infected
141 inflammasome-deficient mice (*Casp1/Casp11*^{-/-}, *Nlr4*^{-/-} and *GasderminD*^{-/-}) and
142 observed that those mice were not protected against *P. aeruginosa* *exoU*⁺, hence
143 suggesting that ExoU-promoted mouse pathology occurs independently from the
144 inflammasome machineries (**Figs. S1A, B**). A hallmark of host cell necrosis is the
145 release of intracellular mediators such as alarmins that contribute to the initiation and
146 the development of an inflammatory reaction, which occurs upon *P. aeruginosa*
147 infection (Aoyagi et al., 2017; Al Moussawi and Kazmierczak, 2014). Therefore, we
148 primarily focused our analysis on alarmin release. We observed a strong ExoU-
149 dependent alarmin production in BALFs 6 h after infection, such as IL-1 family
150 alarmins IL1 α , IL-33 or IL-36 γ (Yang et al., 2017) (**Fig.1C**). In addition, we also
151 detected that *exoU*-expressing *P. aeruginosa* triggered a strong production of
152 phospholipid- and arachidonic acid (aa)-derived mediators such as prostaglandin E2
153 and leukotriene B4, which correlates with the robust phospholipase activity of ExoU
154 (**Fig.1D**) (Machado et al., 2011; Pazos et al., 2017; Saliba et al., 2005). Importantly,
155 BALFs of mice infected with *exoU*-expressing *P. aeruginosa* also exhibited a marked

156 presence of oxidized lipid (by)-products such as isoprostanes (8-iso PGF₂α) or
157 Malondialdehyde (MDA), which suggests that *exoU*-expressing *P. aeruginosa* also
158 drives an exacerbated lipid oxidation response in mice (**Fig.1E**) (da Cunha et al.,
159 2015; Saliba et al., 2006).

160

161 **Lipid peroxidation contributes to ExoU-induced cell necrosis and *P.*** 162 ***aeruginosa* escape from phagocyte-mediated killing**

163 The observation that *exoU*-expressing *P. aeruginosa* infection associates to a lipid
164 peroxidation signature *in vivo*, encouraged us to determine the importance of lipid
165 peroxidation on ExoU-induced cellular necrosis. As *P. aeruginosa* strains that do not
166 express ExoU can promote an NLRC4 inflammasome response in macrophages
167 (Sutterwala et al., 2007), we used mouse Bone-Marrow-Derived Macrophages
168 (BMDMs) that lack *Nlrc4* expression to specifically address the importance of lipid
169 peroxidation on ExoU-dependent cell necrosis. We infected *Nlrc4*^{-/-} primary murine
170 BMDMs with *P. aeruginosa* strains expressing or not expressing ExoU. The
171 pharmacological inhibition of various regulated necrosis pathways (e.g. pyroptosis,
172 necroptosis, apoptosis, parthanatos) showed that only ferrostatin-1, a potent and well
173 characterized inhibitor of phospholipid peroxidation (Skouta et al., 2014), repressed
174 ExoU-dependent cell necrosis (**Figs. 2A, S2A; Movies S1-S6**). In addition, ExoU-
175 induced IL-1α and HMGB1 alarmin release in macrophages was reduced in presence
176 of ferrostatin-1 whereas TNFα levels remained similar (**Fig. 2B**), suggesting that lipid
177 peroxidation contributes to alarmin release in response to ExoU. We noticed that
178 ExoU-triggered ferrostatin-1-sensitive necrosis was not restricted to murine BMDMs
179 as primary human macrophages, the human U937 monocytic cell line, human and
180 murine neutrophils and eosinophils, the human bronchial epithelial (HBEs), A549 or
181 HELA epithelial cells were all sensitive to lipid peroxidation inhibition upon infection
182 with *exoU*-expressing *P. aeruginosa* (**Fig. S2B**). ExoU exhibits a calcium-
183 independent phospholipase A₂-like activity (Dessen, 2000). Hence, we transfected
184 recombinant ExoU protein (rExoU) or its enzymatically inactive mutant ExoU^{S142A}
185 (Tamura et al., 2004) in WT BMDMs and monitored for cell necrosis. Only
186 macrophages transfected with active ExoU underwent to cell death, a process that
187 was inhibited by the use of ferrostatin-1 or the phospholipase inhibitor MAFP (**Fig.**
188 **2C**). In line, we found that ferrostatin-1 itself did not alter bacterial growth or ExoU

189 secretion (**Figs. S2C, D**), suggesting that ferrostatin-1 does not directly alter bacterial
190 physiology nor expression/secretion of ExoU. Upon phospholipase activation
191 arachidonic acid release can be metabolized and oxidized by various cellular
192 enzymes, including cyclooxygenases 1 and 2 (COX1, COX2), lipoxygenases (ALOX5
193 and ALOX12/15 in mice) or cytochrome p450 (CYPs) enzymes. Therefore, we
194 transfected recombinant ExoU in WT, *Alox5^{-/-}* or *Alox12/15^{-/-}* BMDMs in presence or
195 absence of various COX, CYP or different lipid peroxidation inhibitors (α-tocopherol,
196 liproxstatin-1, Resveratrol, ferrostatin-1). Although we observed that all lipid
197 peroxidation inhibitors have a strong inhibitory impact on cell death, cyclooxygenase,
198 cytochrome P450 or lipoxygenase targeting did not interfere with ExoU-dependent
199 cell necrosis, hence suggesting that those enzymes do not regulate lipid-
200 peroxidation-dependent cell necrosis upon ExoU exposure (**Fig. 2D**). Importantly, we
201 also observed that ferrostatin-1 delayed ExoU-induced cell necrosis, suggesting that
202 either the phospholipase activity of ExoU promotes lipid peroxidation-independent
203 cell death or that the inhibitory effect of ferrostatin-1 is unstable over time (**Fig. 2E**).
204 Finally, we evaluated if the inhibition of lipid peroxidation would modulate
205 macrophage and neutrophil microbicidal response upon *exoU*-expressing *P.*
206 *aeruginosa* infection. We observed that ferrostatin-1 strongly improved both
207 macrophage and neutrophil microbicidal activities to a level close to those observed
208 in response to *exoU*-deficient *P. aeruginosa* (**Fig. 2F**), hence suggesting that *P.*
209 *aeruginosa* ExoU relies on lipid peroxidation-dependent cell necrosis to escape from
210 phagocyte attack. Together, our results suggest that host cell lipid peroxidation is
211 important for ExoU-induced host cell necrosis and release of alarmins.

212

213 **Lipid peroxidation fuels ExoU phospholipase activity**

214 Lipid-peroxidation requires reactive oxygen species (ROS), such as H₂O₂, that can
215 oxidize various phospholipids (Dixon et al., 2012). Therefore, we evaluated the ability
216 of ExoU to induce ROS-dependent lipid peroxidation in macrophages. Although we
217 observed that, 30 minutes after transfection, ExoU but not its catalytically inactivated
218 mutant ExoU^{S142A}, triggered an acute ROS production in BMDMs, we surprisingly
219 failed to detect a robust lipid peroxidation accumulation as measured by the C11
220 Bodipy probe (**Figs. 3A, S3A**). As control, the well-known lipid peroxidation inducer
221 Cumene hydroperoxide (CuOOH) promoted cellular lipid peroxidation (**Fig. 3A**)

222 (Lovatt et al., 2020). In contrast, we observed that basal lipid peroxidation in cells
223 was reduced upon ExoU transfection, a process that was further strengthened in
224 presence of ferrostatin-1 (**Fig. 3A**).

225 These results suggest that, instead of promoting pathological lipid peroxidation, ExoU
226 might actually use cellular lipid peroxidation to promote cell necrosis. To this regard,
227 various host phospholipase A2 enzymes have been described to specifically cleave
228 and remove peroxidised phospholipids from membranes (Beatty et al.; Beharier et
229 al., 2020; Lu et al., 2019). To address this hypothesis, we performed a redox
230 phospholipidomic approach to determine if ExoU could interfere with the endogenous
231 levels of peroxidised phospholipids. We used a 45 min time-point to perform our
232 experiments, as a point where plasma membrane permeabilization (propidium uptake
233 monitoring) is not observed. This design excludes the possibility that a decrease in
234 peroxidised phospholipids is due to cell necrosis induced by ExoU (**Fig. S3C**). We
235 observed that *exoU*-treated macrophages had a decrease in peroxidised
236 phospholipids as measured by the reduction in hydroperoxil (-OOH)- and hydroxyl (-
237 OH)-phosphoinositols (PIs)/- phosphoserines (PSs) and - phosphocholines (PCs)
238 with arachidonic acid (C20:4/C22:4) acid side chains (**Figs. 3B, S3B**).

239 In cells, peroxidised phospholipids are detoxified by various factors, one of the most
240 important being the ferroptosis regulator glutathione peroxidase 4 (GPX4) (Dixon et
241 al., 2012). Consequently, the use of pro oxidant molecules or *Gpx4* genetic
242 inactivation both induce a strong accumulation of various peroxidised phospholipids
243 in cell membranes (Dixon et al., 2012). Therefore, we hypothesized that
244 prestimulation of macrophages with non-cytotoxic doses of the lipid peroxidation
245 inducer Cumene hydroperoxide (20µM, 1h) might sensitize cells to ExoU-induced cell
246 necrosis. We transfected recombinant *exoU* in WT BMDMs in presence or absence
247 of non-toxic doses of the pro-oxidant Cumene hydroperoxide (CuOOH, 20µM, 1h)
248 (Lovatt et al., 2020). Although CuOOH promoted lipid peroxidation but not BMDM cell
249 death, *exoU* transfection specifically induced an increased cell necrosis in CuOOH-
250 primed BMDMs, a process that was inhibited by the use of ferrostatin-1 (**Figs. 3C, D**).
251 In agreement with this result, we measured a strong decrease in lipid peroxidation in
252 CuOOH-primed cells transfected with *exoU*, confirming that ExoU efficiently targeted
253 lipid peroxides induced by CuOOH (**Figs. 3C, D**). Finally, using Crispr-Cas9, we
254 generated *Gpx4*^{-/-} immortalized BMDMs (**Fig. S3D**). As previously observed by others

255 in other cell lines (Friedmann Angeli et al., 2014; Kagan et al., 2017), *Gpx4*^{-/-}
256 immortalized BMDMs exhibited increased basal levels of peroxidised lipids (**Fig.**
257 **S3E**). Therefore, *exoU* transfection triggered faster cell death of *Gpx4*^{-/-} macrophages
258 than their WT counterpart, suggesting that lipid peroxidation of cells enhances ExoU-
259 dependent toxicity (**Figs. 3E, S3D, E**).

260 Upon phospholipid peroxidation, arachidonic acid-containing phospholipids from
261 isoprostanes, potent intra- and extra-cellular mediators (Bochkov et al., 2010; Tyurina
262 et al., 2019). Once formed, these isoprostanes are released from phospholipids by
263 the action of phospholipases (Bochkov et al., 2010; Tyurina et al., 2019). Therefore,
264 we reasoned that if ExoU targets peroxidised phospholipids, this would promote
265 ExoU phospholipase-dependent release of endogenous pre-formed isoprostanes.
266 Accordingly, the release of the 8-PGF2 α isoprostane was specifically induced by
267 ExoU in WT macrophages, a process that was further amplified by the co treatment
268 of cells with non-toxic concentrations of Cumen hydroperoxide (CuOOH 20 μ M, 1 h)
269 and ExoU (**Fig. 3F**). Of importance, ferrostatin-1 strongly inhibited ExoU- and
270 ExoU/CuOOH-induced 8-PGF2 α release (**Fig. 3F**). In addition, we also detected that
271 in CuOOH-primed macrophages, the amount of arachidonic acid-derived eicosanoids
272 leukotriene B4 and prostaglandin E2, which are an indirect indication of the
273 phospholipase activity of ExoU, were also strongly increased after the exposure to
274 ExoU, hence suggesting that ExoU-targeted peroxidised phospholipids might
275 increase its phospholipase activity toward all phospholipids (peroxidized or not) (**Fig.**
276 **S3F**). Consequently, we measured the phospholipase activity of ExoU in cell lysates
277 where we chemically induced non-lethal lipid peroxidation with Cumene
278 hydroperoxide (CuOOH, 20 μ M) for 1 h or not. We observed that in CuOOH-primed
279 cell lysates, ExoU exhibited a stronger activity than in unprimed samples after 4 h of
280 incubation (**Fig. 3G**). Importantly, after 18 h incubation, we observed the same
281 accumulation of hydrolysed substrate in CuOOH-primed and unprimed samples,
282 which suggests that lipid peroxidation exacerbates the early activation of ExoU (**Fig.**
283 **3G**). As control, ExoU^{S142A}- treated cell lysates did not show a significant
284 phospholipase activity induction, suggesting that we mostly measured the PLA2
285 activity from ExoU, but not from cellular phospholipases (**Fig. 3G**). Finally, we aimed
286 at challenging our findings by determining if other toxic phospholipases also had a
287 similar activation pattern to ExoU. Hence, we transfected macrophages with the

288 closely related patatin-like phospholipase A2 from *Burkholderia thailandensis*
289 (ExoU^{BitU}) (Anderson et al., 2015). We observed that recombinant ExoU^{BitU}
290 transfection induced BMDMs necrosis, a process that was exacerbated by CuOOH
291 priming and inhibited by the use of ferrostatin-1, suggesting that ExoU^{BitU} also follows
292 a pattern involving host cell lipid peroxidation (**Fig. 3H**). Altogether, our results
293 suggest a surprising mechanism by which ExoU exploits cellular lipid peroxidation to
294 trigger necrosis, a process that can be extended to the action of *B. thailandensis*
295 ExoU^{BitU}-related phospholipase.

296

297 **Ferrostatin-1 improves mouse resistance to infection by *exoU*-expressing *P.*** 298 ***aeruginosa***

299 ExoU-induced necrosis promotes host lung pathology, which leads to a sepsis like
300 response as well as respiratory failure syndrome. Therefore, we hypothesized that
301 ferrostatin-1 use could protect mice against *exoU*-expressing *P. aeruginosa*.
302 Intranasal infection of mice using *P. aeruginosa* *exoU*⁺ showed that mice
303 intraperitoneally pre-treated with ferrostatin-1 (6 h before infection, 6mg.k⁻¹) had
304 diminished bacterial loads in BALFs, lungs and spleen. Ferrostatin-1 pre-treatment
305 did not significantly modify bacterial loads of *exoU*-deficient bacteria, suggesting that
306 ferrostatin-1 mainly modulates ExoU-dependent processes in mice (**Fig. 4A**).
307 Similarly, ferrostatin-1 also attenuated ExoU-dependent alarmin release (e.g. IL-36γ,
308 IL33, IL1α) and the level of oxidized lipids (isoprostanes, MDA) in the BALs (**Fig. 4B,**
309 **C**). Additionally, evaluation of the cellular contents in BALFs showed that ferrostatin-1
310 significantly protected a pool of alveolar macrophage upon *P. aeruginosa* challenge
311 simultaneously decreasing the number of recruited neutrophils, eosinophils and
312 monocytes (**Figs. 4D, S4A**). Although a pathological function of recruited immune
313 cells such as neutrophils is probable, we hypothesize that ferrostatin-1-inhibited
314 resident alveolar macrophage death in response to *exoU*-expressing *P. aeruginosa*
315 might confer an improved immune protection characterized by lower immune cell
316 recruitment and lower tissue damages. Regarding this, lung histological observations
317 showed that the inflammatory status of mice infected with non-lethal doses of ExoU-
318 expressing *P. aeruginosa* (1.10⁵ CFUs) was improved in presence of ferrostatin-1
319 (**Fig. 4E**). Next, we addressed survival upon ExoU-expressing *P. aeruginosa*
320 challenge. We observed that ferrostatin-1-treated mice (4-6 h before infection, 6mg.k⁻¹

321 ¹) had an improved survival rate than those treated with PBS after 40 h after infection
322 (**Fig. 4F**). We validated that ferrostatin-1 specifically protected mice against ExoU-
323 induced pathology as ferrostatin-1-treated mice did not show enhanced protection
324 (survival) against ExoU-deficient *P. aeruginosa* (**Fig. 4F**). Finally, we aimed
325 to evaluate if *P. aeruginosa* ExoU would trigger pathological lipid peroxidation-
326 dependent cell necrosis in human bronchial organoids. Organoids were derived from
327 normal lung tissue adjacent to tumors obtained from patients undergoing lung
328 resection due to non-small cell lung carcinoma (NSCLC). Live cell imaging of
329 organoids microinjected with *P. aeruginosa* showed that ExoU triggered complete
330 organoid collapse (**Fig. 4G; Movies S7-S12**). Importantly, ferrostatin-1 strongly
331 attenuated *P. aeruginosa*-dependent organoid damages (**Fig. 4G; Movies S7-S12**).
332 Altogether, our results identified lipid peroxidation as a pathological mechanism
333 induced by the *P. aeruginosa* ExoU phospholipase both in mice and in human
334 bronchial organoids.

335

336

337

338

339

340

341

342

343

344

345

346

347

348

349

350

351 **Discussion**

352 As a preferential extracellular pathogen, *P. aeruginosa* uses its Type 3-Secretion
353 System (T3SS) to inject virulence factors (Exo S, T, Y and U), allowing bacterial
354 escape from phagocytic uptake and killing. Although *exoS*-expressing *P. aeruginosa*
355 strains associate to the development of chronic infections, *exoU*-expressing *P.*
356 *aeruginosa* triggers acute deadly infections that associate with a strong oxidative
357 imbalance. In this study, we describe that endogenous basal lipid peroxidation
358 contributes to ExoU-dependent cellular toxicity and mouse pathology. Though we do
359 not exclude that *in vivo*, lipid peroxidation might play various pathological roles that
360 go beyond the sole regulation of cell necrosis, such processes appear to be linked to
361 ExoU expression. In this context, previous studies showed that ExoU promotes
362 production of the platelet-activating factor or the 8-PGF₂α isoprostane, two oxidized
363 lipids (da Cunha et al., 2015). In addition, ExoU directly promotes a strong release of
364 arachidonic acid from phospholipids. Enzymes such as cytochrome
365 P450/COXs/LOXs can enzymatically produce oxygenated arachidonic products such
366 as prostaglandin E₂/leukotriene B₄ involved in pathological signalling pathways upon
367 *P. aeruginosa* infection (Machado et al., 2011; Sadikot et al., 2007; Saliba et al.,
368 2005). However, results from others and ours mostly suggest that, taken individually,
369 those enzymes only play a negligible role in ExoU-induced cell necrosis (Machado et
370 al., 2011; Sadikot et al., 2007; Saliba et al., 2005).

371 Although controlled phospholipid peroxidation is of importance for the cells to perform
372 various processes such as efferocytosis through the engagement of peroxidised-PS,
373 mitochondria-dependent apoptosis through cardiolipin peroxidation, signal
374 transduction through peroxidised PC-derived lipids, unrestricted accumulation of
375 peroxidised PEs drives ferroptosis (Bochkov et al., 2010; Tyurin et al., 2014; Tyurina
376 et al., 2019). Specifically, ferroptosis is thought to be a constitutively activated form of
377 cell death that is kept under control through the activity of endogenous regulators of
378 lipid peroxidation such as GPX4, FSP1-mediated coQ10 production, α-tocopherol
379 (vitamin E). In addition, the host cellular calcium (Ca²⁺)-independent PLA2γ, the
380 peroriredoxin Prdx6 PLA2 or the PLA2G6 (Ca²⁺-independent PLA2β) can cleave and

381 remove preferentially peroxidised phospholipids, hence contributing to phospholipid
382 peroxide detoxification (Beharier et al., 2020; Kinsey et al., 2008; van Kuijk et al.,
383 1987; Lu et al., 2019; Miyamoto et al., 2003; Sevanian et al., 1988; Yedgar et al.,
384 2006). The activity of those phospholipases is tightly regulated by various cellular
385 systems (e.g. ROS levels, calcium fluxes, phospholipid composition) that ensure an
386 optimal but not dysregulated phospholipid cleavage (Yedgar et al., 2006). To this
387 regard, our findings that cellular phospholipid peroxidation is a strong enhancer of
388 ExoU-induced pathological necrosis appears in first view counter intuitive. In this
389 context, we envision that, as a virulence factor, ExoU activity does not follow host
390 regulation and uses host peroxidised phospholipids to boost its patatin-like A2
391 phospholipase activity allowing to aberrantly target and cleave host (peroxidised)
392 phospholipids. Consequently, the use of lipid peroxidation inhibitors such as
393 resveratrol, liproxstatin-1 or ferrostatin-1 attenuates the potency and the speed of
394 ExoU-induced cell necrosis. This offers a key time window for macrophage and
395 neutrophil-mediated bacterial uptake and killing. To the contrary, lipid peroxidation
396 accumulation upon *Gpx4* removal or oxidant stress enhances ExoU-induced cellular
397 necrosis. It is intriguing that endogenous peroxidised phospholipids favour ExoU-
398 induced cell necrosis, suggesting that ExoU-expressing strains of *P. aeruginosa* take
399 advantage of the host ferroptosis pathways to maximally damage host tissues.
400 Hence, studying the importance of additional regulators of ferroptosis such as the
401 cytochrome P450 oxidoreductase or the ACSL and LPCAT acyl transferases on
402 ExoU-dependent toxicity warrants further investigations (Doll et al., 2017).

403 Phospholipases are also present in venoms or various microbial pathogens (e.g. *M.*
404 *tuberculosis*, *L. monocytogenes*, *S. pyogenes*) and can also promote fast cell
405 necrosis (Flores-Díaz et al., 2016; Hiu and Yap, 2020; Sitkiewicz et al., 2007).
406 Conversely, we extended our findings to the ExoU closely related ExoU^{BTU}
407 phospholipase from *B. thailandensis*. Remarkably, snake, scorpion or spider venoms
408 are a complex mixture of various components, including the L-amino acid oxidase,
409 able to generate H₂O₂-driven lipid peroxidation, and secreted phospholipases able to
410 cleave phospholipids (Hiu and Yap, 2020). In this context, it is tempting to speculate
411 that venoms have all components necessary to mediate cell damage in a complex
412 single-injection mixture. L-amino acid oxidase-induced lipid peroxidation might work
413 with venom PLA2 to optimize phospholipid cleavage and subsequent cell necrosis.

414 Related to this, Sevanian and colleagues made pioneer observations that the PLA2
415 activity from the snake *Crotalus adamanteus* is exacerbated in contact of liposomes
416 constituted of peroxidised phospholipids, a process that is thought to be due to the
417 better accessibility of the sn2-peroxidized fatty acid to phospholipase (Sevanian et
418 al., 1988). Whether ExoU and its relatives follow a similar pathway of activation will
419 be studied in future studies.

420 In a broader point of view, it is interesting to note that phospholipases can promote
421 allergic shock associated with a strong release of the allergic alarmin interleukin-33
422 (Palm et al., 2013), a signature we also observed in mice infected with ExoU-
423 expressing *P. aeruginosa*. Should lipid peroxidation be involved in IL33-driven allergy
424 or asthma in response to phospholipases or other allergens (e.g. proteases) (Cayrol
425 et al., 2018) will require additional study.

426 Understanding the mechanisms of regulated cell necrosis and their physio-
427 pathological consequences is currently driving intensive research and debates. While
428 the importance of lipid peroxidation in antigen presentation, anti-cancer treatments or
429 in exacerbating neurodegenerative diseases becomes more and more clear, its
430 function in infectious diseases remains less studied. Regarding this, Dar et al.,
431 recently described that, upon chronic infection, secreted *P. aeruginosa* lipoxygenase
432 (loxA) could sensitize cells to lipid peroxidation-induced ferroptosis (Dar et al., 2018).
433 In addition, Kain and colleagues recently linked regulation of host lipid peroxidation
434 and ferroptosis to restriction of liver-stage malaria, which suggests that host
435 peroxidised phospholipids might play yet unsuspected functions in immunity or
436 susceptibility to various pathogens (Kain et al., 2020). Thus, our findings that the
437 bacterial patatin-like phospholipase A2 ExoU contributes to pathology by exploiting
438 target cells lipid peroxidation adds an additional piece of significance for the role of
439 lipid peroxidation in infectious diseases but also offers novel insights to target host
440 lipid peroxidation pathways in the frame of infectious diseases.

441

442

443

444

445

446

447 **ACKNOWLEDGEMENTS**

448 *Alox5^{-/-}* and *Alox12/15^{-/-}* mice came from Agnes Coste (Univ. of Toulouse, France).
449 *Nlrc4^{-/-}* mice were provided by Clare E. Bryant and generated by Millenium, *GsdmD^{-/-}*
450 *^{-/-}* mice came from P. Broz (Univ of Lausanne), and *Casp1^{-/-}/ Casp11^{-/-}* came from
451 B. Py (ENS Lyon, France) and were generated by Junying Yuan (Harvard Med
452 School, Boston, USA). Dara Frank provided essential plasmids, protocols and
453 advices for recombinant phospholipase production and purification. Phospholipid
454 redox lipidomic experiments were performed by Cayman Chemical Company (Ann
455 Arbor, USA). Authors also acknowledge the animal facility and Cytometry/microscopy
456 platforms of the IPBS institute. This project was funded by grants from the National
457 Research Agency (ANR, Endiabac), FRM “Amorçage Jeunes Equipes”
458 (AJE20151034460), ERC StG (INFLAME 804249) and ATIP-Avenir program to EM,
459 from National Research Agency (ANR, MacGlycoTB) to YR, from the European
460 Society of Clinical Microbiology and Infectious Diseases (ESCMID, 2020) to RP, from
461 the Van Gogh Programme to IPBS-M4i institutes, from Invivogen-CIFRE
462 collaborative PhD fellowship to MP and from Mali and Campus France cooperative
463 agencies to SB. The authors acknowledge Ida Rossi, Ines Lakehal and David Péricat
464 for manuscript reading and implementing.

465

466 **AUTHOR CONTRIBUTIONS**

467 SB, RP and EM designed the experiments. SB, RP and EM wrote the manuscript. SB
468 and RP performed the experiments with the help of SLI, MP, AH, KS, EE, PJB, EN,
469 AB, CB, NI, AM, YR and CC. RP and EM supervised the entire study. LL, AC, IA,
470 DWF, HC and PJP provided essential tools, reagents and expertise to conduct the
471 project.

472

473 **CONFLICT OF INTEREST**

474 Authors have no conflict of interest to declare.

475

476

477

478 **FIGURE LEGENDS**

479

480 **Figure 1: ExoU-dependent lung pathology in mice associates to an alarmin and** 481 **peroxidized lipid signature**

482 **(A)** Survival of WT mice intranasally infected (n=7 animals per condition) with 5.10^5
483 CFUs of *P. aeruginosa* PP34 or its isogenic mutant PP34^{exoU-}. Graphs represent one
484 experiment (8 mice/group) out of three independent *in vivo* experiments. Log-rank
485 Cox-Mantel test was used for survival comparisons. ***p ≤ 0.001

486 **(B)** Bronchoalveolar (BAL), lung, blood and spleen bacterial loads from WT mice
487 (n=8) 18 hours after intranasal infection with 5.10^5 CFUs of *P. aeruginosa* PP34 or its
488 isogenic mutant PP34^{exoU-}. Graphs represent one experiment (8 mice/group) out of
489 three independent *in vivo* experiments. **p ≤ 0.01, Mann-Whitney analysis test.

490 **(C)** Alarmin levels in bronchoalveolar fluids (BALFs) from WT mice (n=8) 6 hours
491 after intranasal infection with 5.10^5 CFUs of *P. aeruginosa* PP34 or its isogenic
492 mutant PP34^{exoU-}. Graphs represent one experiment (8 mice/group) out of three
493 independent *in vivo* experiments; *p ≤ 0.05; **p ≤ 0.01, Mann-Whitney analysis test.

494 **(D)** Prostaglandin E2 (PGE2) and Leukotriene B4 (LTB4) levels in bronchoalveolar
495 fluids (BALFs) from WT mice (n=8) 6 hours after intranasal infection with 5.10^5 CFUs
496 of *P. aeruginosa* PP34 or its isogenic mutant PP34^{exoU-}. Graphs represent one
497 experiment (8 mice/group) out of three independent *in vivo* experiments; **p ≤ 0.01,
498 Mann-Whitney analysis test.

499 **(E)** Peroxidized lipid product (isoprostanes and MDA) levels in bronchoalveolar fluids
500 (BALFs) from WT mice (n=8) 6 hours after intranasal infection with 5.10^5 CFUs of *P.*
501 *aeruginosa* PP34 or its isogenic mutant PP34^{exoU-}. Graphs represent one experiment
502 (8 mice/group) out of three independent *in vivo* experiments; *p ≤ 0.05; **p ≤ 0.01,
503 Mann-Whitney analysis test.

504 Data information: Data shown as means (**Graphs B-E**) and are representative of one
505 experiment performed three times; * $p \leq 0.05$; ** $p \leq 0.01$, *** $p \leq 0.001$, Mann-Whitney
506 analysis test (**B-E**) and log-rank Cox-Mantel test for survival comparisons (**A**).

507 **Figure 2: Lipid peroxidation inhibition delays ExoU-induced cell necrosis**

508 Otherwise specified, cells were infected with an MOI of 0.5 of *P. aeruginosa* PP34,
509 PP34^{exoU-} or PP34^{exoUS142A} for various times. *** $p \leq 0.001$, T-test with Bonferroni
510 correction.

511 **(A, B)** Measure of LDH and alarmin/cytokine release in *Nlrc4*^{-/-} BMDMs infected with
512 PP34 or PP34^{exoU-} in presence of Z-VAD (40 μ M), olaparib (10 μ M), Necrostatin-1s
513 (Ne1s, 40 μ M) or Ferrostatin-1 (Fe1, 10 μ M) for 2 hours. *** $p \leq 0.001$, T-test with
514 Bonferroni correction.

515 **(C)** Measure of LDH release in WT BMDMs transfected with recombinant ExoU
516 (100ng), in presence of MAFP (50 μ M) or Ferrostatin-1 (Fe1, 10 μ M) for 3 hours. *** p
517 ≤ 0.001 , T-test with Bonferroni correction.

518 **(D)** Heat map representing measure of LDH release in WT, *ALOX5*^{-/-} and *ALOX12/15*
519 BMDMs transfected with recombinant ExoU in presence/absence of Cox1 inhibitor
520 (Ketorolac Tromethamine, 10 μ M), Cox2 inhibitor (NS 398, 25 μ M), Cyp450
521 epoxygenase activity inhibitor (PPOH, 10 μ M), phospholipase inhibitor MAFP (50 μ M)
522 or lipid peroxidation inhibitors Ferrostatin-1 (Fe1, 20 μ M), Resveratrol (5 μ M),
523 Liproxstatin-1 (30 μ M), α -Tocopherol (20 μ M) for 2 hours. The heat map shows the
524 mean of three combined independent experiments, each performed in triplicate.

525 **(E)** Time course measure of plasma membrane permeabilization using propidium
526 iodide incorporation in *Nlrc4*^{-/-} BMDMs infected with PP34, PP34^{exoU-} or PP34^{exoUS142A}
527 in presence of Ferrostatin-1 (Fe1, 20 μ M). *** $p \leq 0.001$, T-test with Bonferroni
528 correction.

529 **(F)** Microbicidal activity of macrophages (5h) and neutrophils (3h) after infection with
530 *P. aeruginosa* *exoU*⁺ and *exoU* (MOI 0.5) in presence/absence of ferrostatin-1
531 (10 μ M). *** $p \leq 0.001$, T-test with Bonferroni correction.

532

533 Data information: Data are represented as means \pm SEM (graphs A- F) from n = 3
534 independent pooled experiments; ***P \leq 0.001 for the indicated comparisons using t-
535 test with Bonferroni correction.

536

537 **Figure 3: ExoU-induced cell death involves ROS-induced lipid peroxidation but**
538 **proceeds in a ferroptosis independent manner**

539 **(A)** Cytometry detection and quantification of (phosphor)lipid peroxidation using the
540 probe C11-bodipy in WT BMDMs treated with CuOOH (20 μ M) or transfected with
541 rExoU (500ng) or its catalytically dead mutant rExoU^{S142A} (500ng) for 1 hour in
542 presence or absence of Ferrostatin-1 (20 μ M). Sample were acquired using
543 FACSCalibur™ (BD). The graphs shows the mean \pm -SEM of one experiment
544 performed in triplicate out of three independent experiments. **P \leq 0.001, ***P \leq 0.001
545 for the indicated comparisons using t-test with Bonferroni correction.

546 **(B)** (Redox) lipidomic analysis of phospholipid peroxidation in BMDMs transfected
547 with recombinant ExoU or its catalytically dead mutant ExoU^{S142A} for 45 minutes.
548 Each value is standardized to the corresponding phospholipid content shown in **(Fig**
549 **S3B)**. The heat map shows the mean of one experiment performed in triplicate.

550 **(C)** Cytometry detection and quantification of (phosphor)lipid peroxidation using the
551 probe C11-bodipy in WT BMDMs pre-treated or not for 1 hour with CuOOH (20 μ M) in
552 presence or absence of Ferrostatin-1 (20 μ M) and then transfected with rExoU
553 (500ng) for 1 hour. Sample were acquired using FACSCalibur™ (BD). The graphs
554 shows the mean \pm -SEM of one experiment performed in triplicate out of three
555 independent experiments. *P \leq 0.05, **P \leq 0.001, for the indicated comparisons using
556 t-test with Bonferroni correction.

557 **(D)** Measure of LDH release in WT BMDMs pre-treated or not for 1 hour with CuOOH
558 (20 μ M) in presence or absence of Ferrostatin-1 (20 μ M) and then transfected with
559 rExoU (500ng) for 3 hours. ***p \leq 0.001, T-test with Bonferroni correction.

560 **(E)** Time course measure of plasma membrane permeabilization using propidium
561 iodide incorporation in immortalised WT and *Gpx4*^{-/-} BMDMs transfected with rExoU
562 (500ng) for 7 hours. ***p \leq 0.001, T-test with Bonferroni correction.

563 **(F)** Measure of 8-iso PGF2 α isprostane in cell supernatant in WT BMDMs pre-treated
564 or not for 1 hour with CuOOH (20 μ M) in presence or absence of Ferrostatin-1 (20 μ M)
565 and then transfected with rExoU (500ng) for 3 hours. ***p \leq 0.001, T-test with
566 Bonferroni correction.

567 **(G)** ExoU phospholipase activity determination in WT BMDM lysates pre-treated or
568 not with CuOOH (20 μ M, 1hour). 100 pmols of ExoU were used and phospholipase
569 hydrolysis rate (nmoles of substrate hydrolysed/nmole of ExoU) was measured after
570 4 h and 16 hours. ***p \leq 0.001, T-test with Bonferroni correction.

571 **(H)** Measure of LDH release in WT BMDMs primed or not with CuOOH (20 μ M,
572 1hour) in presence or absence of ferrostatin-1 (20 μ M) and transfected for 3 hours
573 with 5 μ g of rExoU^{BtU} or 500ng rExoU. ***p \leq 0.001, T-test with Bonferroni correction.

574

575 Data information: Data are plotted as means \pm SEM (**E-H**) from n = 3 independent
576 pooled experiments; ***P \leq 0.001 for the indicated comparisons using t-test with
577 Bonferroni correction.

578

579 **Figure 4: Ferrostatin-1 protects mice against ExoU-induced lung pathology**

580 **(A)** Bronchoalveolar (BAL), lung and spleen bacterial loads from WT mice
581 (n=7/group) 18 hours after intranasal infection with 5.10⁵ CFUs of *P. aeruginosa*
582 PP34 or its isogenic mutant PP34^{exoU-}. When specified, mice were intraperitoneally
583 pretreated with ferrostatin-1 (6mg.k⁻¹ or PBS) 4 hours before intranasal infection.
584 Graphs represent one experiment (7 mice/group) out of three independent *in vivo*
585 experiments. **p \leq 0.01, Mann-Whitney analysis test. NS: Not significant

586 **(B, C)** Alarmin and lipid peroxide products levels in bronchoalveolar fluids (BALFs)
587 from WT mice (n=7 mice/group) 6 hours after intranasal infection with 5.10⁵ CFUs of
588 *P. aeruginosa* PP34 or its isogenic mutant PP34^{exoU-}. When specified, mice were
589 intraperitoneally pretreated with ferrostatin-1 (6mg.k⁻¹ or PBS) 4 hours before
590 intranasal infection. Graphs represent one experiment (7 mice/group) out of three
591 independent *in vivo* experiments; *p \leq 0.05; **p \leq 0.01, Mann-Whitney analysis test.

592 **(D)** Immune cell (CD45+) populations in bronchoalveolar fluids (BALFs) from WT
593 mice (n=7 mice/group) 6 hours after intranasal infection with 5.10^5 CFUs of *P.*
594 *aeruginosa* PP34 or its isogenic mutant PP34^{exoU-}. When specified, mice were
595 intraperitoneally treated with ferrostatin-1 (6mg.k⁻¹ or PBS) 4-6 hours before
596 intranasal infection. Graphs represent one experiment (7 mice/group) out of three
597 independent *in vivo* experiments; *p ≤ 0.05; **p ≤ 0.01, Mann-Whitney analysis test.

598 **(E)** Histological observation and scoring of bronchial and lung cellular infiltrations
599 upon *exoU*-expressing *P. aeruginosa* intranasal infection. When specified, mice were
600 intraperitoneally pretreated with ferrostatin-1 (6mg.k⁻¹ or PBS) 4-6 hours before
601 intranasal infection. Stars show the cellular infiltrates. *p ≤ 0.05; Mann-Whitney
602 analysis test.

603 **(F)** Mice survival (n=7 mice/group) 40 hours after intranasal infection with 5.10^5 CFUs
604 of *P. aeruginosa* PP34 or its isogenic mutant PP34^{exoU-}. Mice were intraperitoneally
605 pretreated with ferrostatin-1 (6mg.k⁻¹ or PBS) 4 hours before intranasal infection.
606 Graphs represent one experiment (7 mice/group) out of three independent *in vivo*
607 experiments; **p ≤ 0.01, Log-rank Cox-Mantel test was used for survival
608 comparisons.

609 **(G, H)** Time-lapse microscopy and the associated quantifications of the measure of
610 plasma membrane permeabilization using propidium iodide incorporation in human
611 primary bronchial organoids infected (microinjection) with *P. aeruginosa* expressing
612 *exoU*⁺ or its isogenic mutant (*exoU*) in presence or absence of ferrostatin-1 (40μM)
613 for 15 hours. Data are plotted as means± SEM. ***p ≤ 0.001, T-test with Bonferroni
614 correction.

615 Data information: Data shown as means (**Graphs A-E**) and are representative of one
616 experiment performed three times; *p ≤ 0.05; **p ≤ 0.01, Mann-Whitney analysis test
617 (**A-E**) and log-rank Cox-Mantel test for survival comparisons (**F**).

618

619

620

621

622

623

624

625

626

627

628 **STAR Method**

629 **Table 1:** Resource of reagents used in this study

630 Information and reagents are available upon request to Etienne.meunier@ipbs.fr

REAGENT or RESOURCE	SOURCE	IDENTIFIER
Antibodies		
GPX4, 1/1000	abcam	ab125066
ExoU, 1/1000	Ina Attree/CNRS, France.	(Deruelle et al., 2020)
Gapdh 1/10000	Gentex	GTX100118
Goat anti-Rabbit HRP (1/10000)	Advansta	R-05072-500
Bacterial and Virus Strains		
PAO1	J. Buyck/Univ of Poitiers/France	N.A.
PP34	Ina Attree/CNRS, France.	(Deruelle et al., 2020)
PP34 $exoU$	Ina Attree/CNRS, France.	(Deruelle et al., 2020)
PP34 $exoU^{S142A}$	Ina Attree/CNRS, France.	(Deruelle et al., 2020)
CHA	Ina Attree/CNRS, France.	(Deruelle et al., 2020)
CHAdST	Ina Attree/CNRS, France.	(Deruelle et al., 2020)
CHAdST $exoU^+$	Ina Attree/CNRS, France.	(Deruelle et al., 2020)
PA103	J. Buyck/Univ of Poitiers/France	N.A.
PA103 $exoU$	J. Buyck/Univ of Poitiers/France	N.A.
PA14	J. Buyck/Univ of Poitiers/France	N.A.
PA14 $exoU$	J. Buyck/Univ of Poitiers/France	N.A.
Biological Samples		
Human lung biopsy	Hospital of Toulouse	CHU 19 244 C CNRS 205782

Human blood	EFS	21PLER2017-0035AV02
Chemicals, Peptides, and Recombinant Proteins		
Recombinant ExoU	This study	(Anderson et al., 2015)
Recombinant ExoUS142A	This study	(Anderson et al., 2015)
FCS	Fisher Scientific	16010-159
mMCSF	L929 cell supernatant	NA
HEPES	Fisher Scientific	SH30237.01
Non-essential amino acids	Invitrogen	
ECL Clarity Max Substrate	BioRad	1705060
ECL Clarity Max Substrate	BioRad	1705062
Western Blot Strip Buffer	Diagomics	R-03722-D50
Tris base	euromedex	200923-A
SDS ultra-pure (4x)	Euromedex	1012
Acrylamide / Bisacrylamide 37.5/1 30%	Euromedex	EU0088-B
Temed	Sigma	T9281-25ML
Ammonium persulfate	Sigma	248614-100g
Page Ruler 10-180 kDa	Fisher Scientific	15744052
Triton X-100	Euromedex	2000
DMEM	Fisher Scientific	41965-039
LB	Fisher Scientific	BP1426-2
LB Agar	INVITROGEN	22700025
Roche protease inhibitor cocktail	Sigma	0000000116974980 01
BSA	SIGMA	A9647-100G
Propidium iodide	Invitrogen	P3566
Beads Neutrophils human	Miltenyi biotec	130-104-434
Beads Neutrophils murine	Miltenyi biotec	130-120-337
Kit de coloration bleue et fixable des cellules mortes LIVE/DEAD™ pour excitation UV	ThermoFisher Scientifique	L34961
APC/Cyanine7 anti-mouse CD45 Antibody	BioLegend	103116
PE/Dazzle™ 594 anti-human CD64 Antibody	BioLegend	305032
FITC anti-mouse MERTK (Mer) Antibody	BioLegend	151504
CD170 (Siglec F) Monoclonal Antibody (1RNM44N), Super Bright 780,	eBioscience	78-1702-82
Ly-6G Monoclonal Antibody (1A8-Ly6g), APC	eBioscience	17-9668-82
Brilliant Violet 650™ anti-mouse/human CD11b Antibody	BioLegend	101259
Brilliant Violet 421™ anti-mouse Ly-6C Antibody	BioLegend	128032
PE/Cyanine7 anti-mouse CD11c Antibody	BioLegend	117318
Eosinophil differentiation cocktail (IL-5)	R&D Systems	405-ML-005
Eosinophil differentiation cocktail (SCF)	BioLegend	579706
Eosinophil differentiation cocktail (Flt-3)	BioLegend	550706
Puromycin	ThermoFisher Scientifique	A1113803
G418 (Geneticin)	invivoGen	ant-gn-1

Blasticidin	nvivoGen	ant-bl-1
Cumene hydroperoxide	Sigma-Aldrich	247502-5G
RSL3	Sigma-Aldrich	SML2234
Ferostatin-1	Sigma-Aldrich	SML0583
Liproxstatin-1	Sigma-Aldrich	SML1414
DFO	Sigma-Aldrich	D9533
a-tocopherol	Sigma-Aldrich	258024
MAFP	Sigma-Aldrich	M2689
PPOH	CaymanChem	75770
Cox1 inhibitor	Ab142904 (Abcam)	Ab142904
Cox2 inhibitor	NS 398 (Abcam)	Ab120295
cPLA2 assay kit	Cayman Chemical	765021
CD14+ beads	Miltenyi biotec	130-050-201
RPMI	Fisher Scientific	72400-021
OPTIMEM	Fisher Scientific	31985-04
Z-VAD	Invivogen	tlrl-vad
Olaparib	CaymanChem	10621
Necrostatin-1s	Sigma-Aldrich	N9037 10MG
hMCSF	Miltenyi biotec	170-076-171
Fisher BioReagents™ Lymphocyte Separation Medium-LSM	Fisher Scientific	BP2663500
ExoU	This study	N.A.
ExoUS142A	This study	N.A.
Human bronchial organoid culture reagents		
Advanced DMEM/F12	Invitrogen	12634028
Gibco™ L-Glutamine (200 mM)	Fisher	11500626
Hepes 1 M	Fisher	11560496
Penicillin/Streptomycin	Fisher	11548876
Primocin	Invivogen	ant-pm-1
Basic Media	In house	NA
Rspol	In house	NA
Noggin	In house	NA
B27	Gibco/Invitrogen	17504044
N-Acetylcysteine	Sigma	A9165-5g
Nicotinamide	Sigma	N0636
Y-27632	Cayman	10005583
A83-01	Tocris	2939
SB 202190	Sigma	S7067
FGF-7	Peprtech	100-19
FGF-10	Peprtech	100-26
Critical Commercial Assays		
mIL-1alpha ELISA kit	Fisher Scientific	88-5019-88
mIL-36g ELISA kit	Ray Biotech	ELM-IL36G
LDH Cytotoxicity Detection Kit	Takara	MK401
mTNFalpha ELISA kit	Fisher Scientific	88-7324-22

mIL-33 ELISA kit	Fisher Scientific	88-7333-88
mHMGB1 ELISA kit	Clinisciences	LS-F4040-1
TBAR MDA colorimetric kit	Cayman	10009055
PGE2 EIA Kit	Cayman	514010
LTB4 EIA kit	Cayman	520111
8-PGF2 EIA kit	Cayman	516351
H2DCFDA ROS detecting probe	Invitrogen	D399
C11 bodipy phospholipid peroxide detection probe	Invitrogen	D3861
Experimental Models: Cell Lines		
WT Mouse Bone marrow derived macrophages	This study	
Alox5 ^{-/-} Mouse Bone marrow derived macrophages	This study	
Alox12/15 ^{-/-} Mouse Bone marrow derived macrophages	This study	
Nlrc4 ^{-/-} Mouse Bone marrow derived macrophages	This study	
Casp1 ^{-/-} /Casp11 ^{-/-} Mouse Bone marrow derived macrophages	This study	
GsdmD ^{-/-} Mouse Bone marrow derived macrophages	This study	
WT Mouse bone marrow derived eosinophils	This study	
WT Mouse bone marrow derived neutrophils	This study	
Human blood monocyte derived macrophages	This study	
Human blood neutrophils	This study	
Immortalized WT murine bone marrow derived macrophages	This study	
Immortalized Gpx4 ^{-/-} murine bone marrow derived macrophages	This study	
Human Bronchial epithelial cells	This study	
Human Alveolar epithelial A549 cell line	This study	
Human intestinal epithelial HELA cell line	This study	
Experimental Models: Organisms/Strains		
WT C57Bl6J mice	C. Rivers	
WT C57Bl6N mice	C. Rivers	
Alox5 ^{-/-} C57Bl6 mice	A.Coste	(Lefèvre et al., 2015)
Alox12/15 ^{-/-} C57Bl6 mice	A.Coste	(Lefèvre et al., 2015)
Nlrc4 ^{-/-} C57Bl6 mice	C.Bryant	(Man et al., 2014)
Casp1 ^{-/-} /Casp11 ^{-/-} C57Bl6 mice	B.Py/ Junying Yuan	(Li et al., 1995)
GsdmD ^{-/-} C57Bl6 mice	P.Broz	(Demarco et al., 2020)
Human Bronchial organoids	This study	(Bartfeld and Clevers, 2015; Sachs et al., 2019)
Oligonucleotides		
Guide Crispr mGpx4- Exon1 Forward	Sigma-Aldrich	GGACGCTGCAGA CAGCGCGG
Recombinant DNA		
Plasmid: ExoU	(Anderson et al., 2015)	(Anderson et al., 2015)
Plasmid: ExoUS142A	(Anderson et al., 2015)	(Anderson et al., 2015)
Plasmid: ExoU ^{BTU}	(Anderson et al., 2015)	(Anderson et al., 2015)
LentiGuide-Puro	Feng Zhang lab	Addgene #52963
Lenti-multi-Guide	From Qin Yan	Addgene #85401

pMD.2G	Didier Trono lab	Addgene #12259
p8.91	Didier Trono lab	N.A.
LentiCas9-Blast	Feng Zhang lab	Addgene #52962
Software and Algorithms		
Graph Pad Prism 8.0		
Image J		
Snappgene	GSL Biotech LLC, Chicago, U.S.A	
FlowJO	FlowJo LLC	
Benchling Software		
Other		

631

632 **Mice**

633 *Nlr4^{-/-}*, *Casp1^{-/-}Casp11^{-/-}*, *GsdmD^{-/-}*, *ALOX12/15^{-/-}* and *ALOX5^{-/-}* mice were
634 generated and described in previous studies (Demarco et al., 2020; Lefèvre et al.,
635 2015; Li et al., 1995; Man et al., 2014). Mice were bred at the IPBS (Toulouse,
636 France) animal facilities in agreement to the EU and French directives on animal
637 welfare (Directive 2010/63/EU). Charles Rivers provided WT C57BL/6 mice.

638

639 **Animal infection models**

640 6-10 mice/group were intranasally infected with $5 \cdot 10^5$ Colony Forming Units (CFUs)
641 of *P. aeruginosa* PP34 strain (*ExoU^t*) or its isogenic mutant (*ExoU*) and animal
642 survival was followed over 40-50 hours after infection. When specified, mice were
643 intraperitoneally treated with 100 μ L of PBS or ferrostatin-1 (6mg.k⁻¹) 4-6 hours before
644 intranasal infections with bacterial strains.

645 Regarding bacterial loads assays, 6-10 mice/group were intranasally infected with
646 $2 \cdot 10^5$ bacteria for 24 hours, and Bronchoalveolar (BALs), lung spleen and blood
647 bacterial numbers were evaluated using CFU plating. BAL fluids (BALFs) were also
648 used to address cytokine, alarmin and lipid levels using ELISA, EIA and colorimetric
649 kits. There were no randomization or blinding performed.

650 Animal experiments were approved (License APAFIS#8521-2017041008135771,
651 Minister of Research, France) and performed according to local guidelines (French
652 ethical laws) and the European Union animal protection directive (Directive
653 2010/63/EU).

654

655 **Histological experiments and scoring**

656 Mice were intraperitoneally treated with 100 μ L of PBS or ferrostatin-1 (6mg.k⁻¹) 4-6
657 hours before intranasal infections with sub-lethal doses (2.10⁵ CFUs) of *exoU*-
658 expressing *P. aeruginosa*. 6 hours later, lung tissues were fixed for 48 h in 10%
659 buffered formalin, washed 3 times in ethanol 70% and embedded in paraffin. 5 μ m
660 sections were stained with hematoxylin and eosin (HE). Histopathological scoring
661 from 0 to 3 were attributed based on the severity of peribronchial, perivascular, and
662 interstitial cell infiltration, resulting in a maximum score of 9.

663 **Bacterial cultures**

664 *P. aeruginosa* (PP34, PA103, CHA, PAO1, PA14) bacteria and their isogenic mutants
665 were grown overnight in Luria Broth (LB) medium at 37°C with aeration and constant
666 agitation in the presence or absence of EGTA (10mM) to ensure T3SS expression.
667 Bacteria were sub-cultured the next day by dilution overnight culture 1/50 and grew
668 until reaching an optical density (OD) O.D600 of 0.6 – 1. Bacterial strains and their
669 mutants are listed in Table S1.

670

671 **Bone Marrow-derived Macrophage (BMDMs), Eosinophil (BMDEs) or Neutrophil 672 (BMDNs) isolation and culture.**

673 Murine Bone Marrow-Derived Macrophages (BMDMs) from bone marrow progenitors
674 were differentiated in DMEM (Invitrogen) supplemented with 10% v/v FCS (Thermo
675 Fisher Scientific), 10% v/v MCSF (L929 cell supernatant), 10 mM HEPES
676 (Invitrogen), and nonessential amino acids (Invitrogen) for 7 days as previously
677 described (Eren et al., 2020).

678 Murine Bone Marrow-Derived Eosinophils were differentiated *in-vitro* from bone
679 marrow as previously described (Dyer et al., 2008). cells were resuspended and
680 cultured at 10⁶/mL in RPMI glutamax medium with HEPES containing 20% FBS, 100
681 IU/ml penicillin and 10 μ g/ml streptomycin, 1 mM sodium pyruvate (Life
682 Technologies), and 50 μ M 2-ME (Sigma-Aldrich) supplemented with 100 ng/ml stem
683 cell factor (SCF; PeproTech) and 100 ng/ml FLT3 ligand (FLT3-L; PeproTech) from
684 days 0 to 4. On day 4, the medium containing SCF and FLT3-L was replaced with

685 medium containing 10 ng/ml recombinant mouse (rm) IL-5 (R&D Systems) only.
686 Medium was replaced every 4 days and the concentration of the cells was adjusted
687 each time to 10^6 /ml. After 10 to 14 days of culture, cells were recovered by gentle
688 pipetting and used as Eosinophils in our experiments. Over 95% of cells had the
689 standard phenotype of Eosinophils : CD11b+ Siglec F + after FACS analysis.

690 Murine Bone Marrow-derived Neutrophils were isolated and purified from fresh bone
691 marrows using Anti-Ly-6G micro bead kit (Miltenyi Biotec). Analysis of cell purity by
692 FACS show that over 95% of cells had the standard phenotype of Neutrophils
693 Ly6G+/Ly6C+.

694 2.5×10^5 BMDMs or 1.10^6 BMDEs/BMDNs were seeded in 24 well-plates and infected
695 or exposed to various treatments. Regarding ferroptosis experiments, BMDMs were
696 infected with various bacterial strains of *P. aeruginosa* expressing or not *exoU* at an
697 MOI 0.1-1 for various times. When specified, recombinant microbial phospholipases
698 (10ng-1 μ g) were transfected in BMDMs using Fugene (3 μ l per 1 μ g of transfected
699 protein) for 2-4 hours. Compound-induced ferroptosis was achieved using RSL-3
700 (10 μ M, 8H) or Cumene hydroperoxide (CuOOH, 500 μ M, 3H).

701 When required, BMDMs were pretreated for 2 hours with pharmacological inhibitors
702 necrostatin-1s (40 μ M), Z-VAD (40 μ M), olaparib (10 μ M), ferrostatin-1 (1-40 μ M),
703 MAFP (50 μ M), liproxstatin (30 μ M), α -tocopherol (20 μ M).

704 For all stimulations, cell culture medium was replaced by serum-free and antibiotic-
705 free Opti-MEM medium and triggers were added to the cells for various times.

706

707 **Cell line culture**

708 Immortalized murine bone-marrow derived macrophages have been described
709 previously (Eren et al., 2020). U937 cells were cultured in RPMI glutamax medium
710 containing 10% FBS, 100 IU/ml penicillin and 10 μ g/ml streptomycin, 1 mM sodium
711 pyruvate (Life Technologies), and 50 μ M 2-ME (Sigma-Aldrich). Medium was
712 renewed every 3 days and the concentration of the cells was adjusted each time to
713 5×10^5 /ml. A549, HeLa and HBE cells were cultured in DMEM glutamax medium with
714 HEPES containing 10% FBS, 100 IU/ml penicillin and 10 μ g/ml streptomycin, 1 mM
715 sodium pyruvate (Life Technologies). When the cells reach approximately 90%

716 confluency, cells are detached with Trypsin 0.05% (Gibco), cell suspension is diluted
717 1/10 in fresh medium, and placed back in the incubator for culture.

718

719

720

721 **Purification and generation of human blood neutrophils and monocyte-derived** 722 **Macrophages**

723 Monocytes were isolated from Peripheral Blood Mononuclear Cells (PBMCs) from the
724 buffy coat of healthy donors obtained from the EFS Toulouse Purpan (France) as
725 described previously (Troegeler et al., 2014). Briefly, PBMCs were isolated by
726 centrifugation using standard Ficoll-Paque density (GE Healthcare) (Eren et al.,
727 2020). The blood was diluted 1:1 in phosphate-buffered saline (PBS) pre-warmed to
728 37°C and carefully layered over the Ficoll-Paque gradient. The tubes were
729 centrifuged for 25 min at 2000 rpm, at 20°C. The cell interface layer was harvested
730 carefully, and the cells were washed twice in PBS (for 10 min at 1200 rpm followed
731 by 10 min at 800 rpm) and re-suspended in RPMI-1640 supplemented with 10% of
732 foetal calf serum (FCS), 1% penicillin (100 IU/mL) and streptomycin (100 µg/ml).
733 Monocytes were separated from lymphocytes by positive selection using CD14+
734 isolation kit (Mytenyi biotec). To allow differentiation into monocyte-derived
735 macrophages, cells were cultured in RPMI medium (GIBCO) supplemented with 10%
736 FCS (Invitrogen), 100 IU/ml penicillin, 100µg/ml streptomycin, 10 ng/ml M-CSF for 7
737 days.

738 Human blood neutrophils were isolated from whole blood of healthy donors obtained
739 from the EFS Toulouse Purpan (France). Neutrophils were enriched using
740 MACSxpress Whole Blood Neutrophil Isolation Kit whole blood neutrophil isolation kit
741 (Mytenyi biotec) according to manufacturer instructions. Red blood cells (RBC) were
742 removed by 10 min incubation in RBC Lysis Buffer (BioLegend).

743

744 **Genetic invalidation of *Gpx4* genes in immortalized BMDMs**

745 Targeted genes were knocked-out using the crispr/cas9 system in immortalized
746 BMDMs. Single guide RNAs (sgRNA) specifically targeting *Gpx4* exon1 (for 5'
747 GGACGCTGCAGACAGCGCGG 3' were designed using Benchling tool
748 (Benchling.com), and oligonucleotides were synthesized by Sigma-Aldrich. Crispr
749 guide RNA oligonucleotides were hybridized and subsequently cloned into the vector
750 Lenti-gRNA-Puromycin using BsmBI restriction enzyme (Addgene 52963, Feng
751 Zhang lab). Generated constructs were then transfected in lipofectamine 2000 into
752 HEK293T for 48 hours together with the lentiviral packaging vector p8.91 (Didier
753 Trono lab, EPFL, Switzerland) and the envelop coding VSVg plasmid (pMD.2G,
754 Addgene 12259, Didier Trono lab). Viral supernatants were harvested, filtered on
755 0.45 µm filter and used to infect cells expressing Cas9 (1,000,000 cells/well in 6-well
756 plates. Efficient infection viral particles was ensured by centrifugating cells for 2 h at
757 2900 rpm at 32°C in presence of 8µg/ml polybrene. 48 h later, medium was replaced
758 and Puromycin selection (10µg/mL) was applied to select positive clones for two
759 weeks. Puromycin-resistant cells were sorted at the single cell level by FACS (Aria
760 cell sorter). Individual clones were subjected to western blotting to confirm the
761 absence of targeted proteins.

762

763 **Human bronchial organoid production and maintenance**

764 Airway organoids were derived from lung biopsies as described (Bartfeld and
765 Clevers, 2015; Sachs et al., 2019). Briefly, Human lung tissue was provided by the
766 CHU of Toulouse under the CNRS approved protocols CHU 19 244 C and CNRS
767 205782. All patients participating in this study consented to scientific use of their
768 material. Biopsies (1 mm³) of normal lung tissue adjacent to the tumor obtained from
769 patients who underwent lung resection due to Non-small cell lung carcinoma
770 (NSCLC) were minced and digested with 2 mg ml⁻¹ collagenase (Sigma) on an
771 orbital shaker at 37°C for 1h. The digested tissue suspension was sheared using
772 flamed glass Pasteur pipettes and strained over a 100-µm cell strainer (Falcon). The
773 resultant single cell suspensions were embedded in 10 mg ml⁻¹ of Cultrex growth
774 factor reduced BME type 2 (R & D Systems) and 40µl drops were seeded on
775 Nunclon Delta surface 24-well plates (Thermo Scientific). Following polymerization,
776 500 µl of Advanced DMEM/F12 (Invitrogen) supplemented with 1x L-Glutamine

777 (Fisher Scientific), 10mM HEPES (Fisher Scientific), 100 U ml⁻¹ / 100 µg ml⁻¹
778 Penicillin / Streptomycin (Fisher Scientific), 50 µg ml⁻¹ Primocin (InvivoGen), 10%
779 Noggin (homemade), 10% Rspol (homemade), 1x B27 (Gibco), 1.25mM N-
780 Acetylcysteine (Sigma-Aldrich), 10mM Nicotinamide (Sigma-Aldrich), 5µM Y-27632
781 (Cayman Chemical), 500nM A83-01 (Tocris Bioscience), 1µM SB 202190 (Sigma-
782 Aldrich), 25 ng ml⁻¹ FGF-7 (PeproTech), 100 ng ml⁻¹ FGF-10 (PeproTech) was
783 added to each well and plates transferred to humidified incubator at 37°C with 5%
784 CO₂. The organoids were passaged every 4 weeks.

785

786

787 **Organoid infections**

788 Before infection, 35µl drops of Matrigel (Fisher Scientific) containing organoids were
789 seeded on Nunclon Delta surface 35x10mm Dish (Thermo Scientific) and 2ml of
790 Advanced DMEM/F12 supplemented with 1x L-Glutamine and 10mM HEPES was
791 added to each plate. Depending on the indicated conditions, organoids were
792 pretreated or not with 40µM Ferrostatin-1 for 1hr before infection. Ferrostatin-1 was
793 maintained throughout the experiment. PP34 *exoU* or *exoU*^{S142A} were grown as
794 previously described until reach OD₆₀₀ = 1. Bacterial density was adjusted to OD₆₀₀
795 = 0.0005, and phenol red added at 0.005% to visualize successful microinjection (2).
796 Injected organoids were individually collected and re-seeded into fresh matrix for
797 subsequent analysis. For time-lapse imaging, injected and stimulated organoids were
798 stained with 50 µg ml⁻¹ Propidium Iodide (Thermo Scientific). Images were acquired
799 every 15 minutes for the duration of experiments under an EVOS M7000 (Thermo
800 Scientific) Imaging System (10x, at 37°C with 5% CO₂). Data was analyzed using
801 Fiji/ImageJ.

802

803 **Cell necrosis, alarmin/cytokine and lipid release assays**

804 LDH Cytotoxicity Detection Kit (Takara) was used to determine the percentage of cell
805 lysis. Normalization of spontaneous lysis was calculated as follows: (LDH infected –
806 LDH uninfected)/(LDH total lysis – LDH uninfected)*100.

807 Murine IL-1 α , IL-33, IL-36 α , IL-36 γ , HMGB1, TNF α , cytokine levels in cell
808 supernatants or in BALFs were measured by ELISA listed in resource Table 1.

809 Oxidized lipids isoprostanes, eicosanoids PGE2 and LTB4 were detected in cellular
810 supernatants or BALFs using EIA kits listed in resource Table 1.

811

812 **Plasma membrane permeabilization assays**

813 Cells are plated at density of 1×10^5 per well in 96-well Plates or at 2×10^5 /well in 24-
814 well plates (Corning 356640) in complete culture medium. The following day, medium
815 is replaced by Opti-MEM supplemented with Propidium iodide (100 ng/ml) or SYTOX
816 green (100ng/mL). Pharmacological inhibitors are added 1h before infection. Red
817 (Propidium Iodide) or green (SYTOX) fluorescence are measured in real-time using
818 Clariostar plate reader or an EVOS7000 microscope, both equipped with a 37°C cell
819 incubator.

820

821 **Malondialdehyde (MDA) assays**

822 Malondialdehyde production was addressed using the MDA lipid peroxidation kit
823 according to the manufacturer's instructions (Abcam, ab118970). Cells were lysed
824 using 500 μ l of lysis buffer supplemented with butylated hydroxytoluene. Cell lysates
825 were centrifuged for 10 min at 13,000 g (RCF) and the supernatants were used for
826 MDA assay. TBA solution was added to each replicate, and samples were then
827 incubated at 95°C for 1 hour. 100 μ L of each sample was then processed for
828 fluorometric assay at Ex/Em = 532/553 nm. BAL levels of MDA were normalized to
829 the total protein concentration.

830

831 **Recombinant protein production**

832 Plasmids coding for *exoU*^{BtU}, *exoU* or *exoU*^{S142A} were a kind gift from Dara W.
833 Frank's lab. All recombinant proteins were expressed in BL21(DE3) pLysS strain in
834 LB medium, according to Anderson DM et al. (Anderson et al., 2015). Proteins fused
835 with an N-terminus hexahistidine-tag were purified as previously described with slight
836 modifications. Briefly, after cell harvest, bacteria were lysed by sonication under ice

837 and recombinant proteins were purified by nickel metal affinity chromatography
838 (Takara). After sample concentration, Superose 6 was exchanged for a Superdex
839 200 size exclusion column (GE Healthcare) as a final purification step. Samples were
840 either used fresh or keep at -80°C for long-term storage.

841

842 **Cytometry quantification of immune cells in mice BAL fluids (BALFs)**

843 C57BL/6 mice received an injection of Ferrostatine (6mg/kg) or PBS as control
844 intraperitoneally. 4-6h after, mice were infected by intranasal instillation of 50 µL of
845 PBS containing or not 5×10^6 bacteria (PP34) in presence or absence of Ferrostatine
846 (6mg /kg). 18h after infection, BALFs were collected and quality/quantity of immune
847 cells content was assayed by flow cytometry. Briefly, cells were pelleted (1000 rpm, 5
848 minutes), Red blood cells (RBC) were removed by 10 min incubation in RBC Lysis
849 Buffer (BioLegend), monocytes, macrophages, neutrophils, and eosinophils were
850 subsequently stained with a cocktail of fluorochrome-conjugated antibodies detailed
851 in the material section. Cells were then fixed in 4% PFA before fluorescence
852 associated cell sorting (FACS) analysis using a LSRII instrument. AccuCheck
853 Counting Beads (ThermoFisher) were used to determine absolute cell number. Data
854 analysis and processing were performed using FlowJO software.

855

856 **Cytometry-based Lipid peroxidation or ROS production**

857 To measure lipid peroxidation or ROS production, cells were first washed with PBS
858 1X, and then incubated with either C11-BODIPY(581/591) (ThermoFisher) at 2 µM,
859 or H2DCFDA (ThermoFisher) at 10 µM in Opti-MEM medium for 30 min at 37°C.
860 After three washes with PBS 1X cells are resuspended in Opti-MEM medium and
861 infected in presence or absence of pharmacological inhibitors. After 1-3h of infection,
862 cells are washed with PBS, detached in MACS buffer (PBS-BSA 0,5%-EDTA 2mM)
863 and samples were acquired within one hour using a flow cytometer (BD FORTRESSA
864 LSR II). Data were analysed with FlowJO software (version 10).

865

866 **Immunoblotting**

867 Cell lysate generation has been described previously (Eren et al., 2020). Briefly,
868 proteins were loaded in 12% SDS-PAGE gels and then transferred on PVDF
869 membranes. After saturation for 1 hour in Tris-buffered saline (TBS) supplemented
870 with 0.05% Tween 20 containing 5% non-fat milk (pH8), membranes were exposed
871 with antibodies at 4°C overnight (Table 1). Next day, membranes were washed 3
872 times in TBS 0.1% Tween 20 and incubated with the corresponding secondary
873 antibodies conjugated to horseradish peroxidase (HRP) (Table 1) for 1h at room
874 temperature. Immunoblottings were revealed using a chemiluminescent substrate
875 ECL substrate (Biorad) and images were acquired on a ChemiDoc Imaging System
876 (Biorad). All antibodies and their working concentrations are listed in Table 1.

877

878

879 **(Redox) lipidomic**

880 1 million bone-marrow-derived macrophages were seeded into 6-well plates. Next
881 day, BMDMs were transfected with recombinant ExoU or ExoU^{S142A} proteins
882 (500ng/well) for one hour. Then, supernatant was removed, cells were washed two
883 times in PBS. Finally, 500µL of a cold solution of 50% PBS/50% Methanol was added
884 to cells and samples were transferred to -80°C for storage and subsequent analyses.

885 After thawing, lipids were extracted using a methyl-tert-butyl ether (MTBE)-based
886 liquid-liquid extraction method. Cell suspensions (500 µL in PBS/methanol 1:1, v/v)
887 were thawed on ice before adding 100 µL methanol MeOH containing 50 ng each of
888 the internal standards PC(15:0/18:1-d7), PE(15:0/18:1- d7), PG(15:0/18:1-d7),
889 PI(15:0/18:1-d7) and PS(15:0/18:1-d7) (EquiSPLASH, Avanti Polar Lipids). Samples
890 were then transferred into 8-mL screw-cap tubes, and then 1.125 methanol and 5 mL
891 MTBE were added. After vigorous mixing, samples were incubated at room
892 temperature on a tabletop shaker for 45 min. For phase separation, 1.25 mL water
893 was added, and samples were vortexed and centrifuged for 15 min at 2000 x g. The
894 upper organic phase of each sample was carefully removed using a Pasteur pipette,
895 transferred into an empty glass round-bottom tube, and dried under vacuum in a
896 SpeedVac concentrator. The dried lipid extracts were resuspended in 200 µL HPLC
897 mobile phase A/mobile phase B 3:1 (v/v) for targeted lipidomic analysis of oxidized
898 phospholipids. For LC-MS/MS, using a Sciex ExionLC Integrated System, 20 µL of

899 each lipid extract was injected using Column Kinetex 2.6 μm HILIC 100 \AA 100x2.1
900 mm, Phenomenex and a Flow Rate of 200 $\mu\text{L}/\text{min}$. Then, the analyte-specific m/z
901 transition profile was determined and the area under the peak (ion intensity vs.
902 elution time) was calculated using MultiQuant, Sciex software.

903 Data calculation was performed by doing ratio between the values of “area ratio
904 analyte/internal standard” of each oxidized phospholipid and its non-oxidized
905 phospholipid. The fold induction in oxidized phospholipid was then calculated by
906 doing a ratio between each oxidized ratio and the non-stimulated condition.
907 Accordingly, the unstimulated condition oxidized ratios were 1 or 0 when no
908 peroxidation was detected in any condition.

909

910

911 **Phospholipase activity measurement**

912 Evaluation of ExoU phospholipase activity was performed using the Cayman
913 Chemical cPLA2 kit and performed as previously described with minor modifications
914 (Deruelle et al., 2020). Briefly, 10 μL of a 1mg/mL (160pmols) solution of recombinant
915 ExoU or ExoU^{S142} proteins were mixed in 96-well plates with 10 μL of lysed cell
916 samples and 10 μL of Assay Buffer. Then, samples were incubated for 1 hour at room
917 temperature with 250 μL of substrate solution (1.5 mM arachidonyl
918 thiophosphatidylcholine) and then for additional 4 or 16 hours in dark. Reaction was
919 stopped using 25mM solution of DTNB according to manufacturer instructions and
920 absorbance was detected at 405nm using a Clariostar plate reader. Phospholipase
921 activity of ExoU or ExoU^{S142} was calculated as the hydrolysis rate accordingly to the
922 manufacturer instructions.

923

924 **Ethics statements**

925 The use of human cells was performed under the agreement of the Research Ethical
926 Committee, Haute-Garonne, France. Buffy coats came anonymously by the EFS
927 (établissement français du sang, Toulouse, France). For each donor, a written
928 informed consent was obtained according to the EFS contract agreement n°

929 21PLER2017-0035AV02, according, to “Decret N° 2007-1220 (articles L1243-4,
930 R1243-61)”.

931

932 **Statistical analysis**

933 Statistical data analysis was performed using Prism 8.0a (GraphPad Software, Inc.).
934 We used T-test with Bonferroni correction for comparison of two groups. Data are
935 reported as mean with SEM. Regarding animal experiments, we used Mann-Whitney
936 tests and mouse survival analysis were done using log-rank Cox-Mantel test. P
937 values in figures have the following meaning; NS non-significant and Significance is
938 specified as * $p \leq 0.05$; ** $p \leq 0.01$, *** $p \leq 0.001$.

939

940

941

942 **Supplemental information**

943

944 **Figure S1: ExoU-dependent lung pathology in mice occurs in an** 945 **inflammasome-independent manner**

946 **(A)** Survival of WT, *Casp1^{-/-}/Casp11^{-/-}*, *Nlr4^{-/-}* and *GsdmD^{-/-}* mice intranasally
947 infected (n=6 animals per condition) with $5 \cdot 10^5$ CFUs of *P. aeruginosa* PP34. Graphs
948 represent one experiment (6 mice/group) out of three independent *in vivo*
949 experiments. NS: Not significant using Log-rank Cox-Mantel test for survival
950 comparisons.

951 **(B)** Bronchoalveolar (BAL) and lung bacterial loads from WT, *Casp1^{-/-}/Casp11^{-/-}*,
952 *Nlr4^{-/-}* and *GsdmD^{-/-}* mice (n=6) 18 hours after intranasal infection with $5 \cdot 10^5$ CFUs
953 of *P. aeruginosa* PP34. Graphs represent one experiment (6 mice/group) out of three
954 independent *in vivo* experiments. NS: Not significant using Mann-Whitney analysis
955 test.

956

957 **Figure S2: Lipid peroxidation contributes to ExoU-induced necrosis in various**
958 **cell types**

959 **(A)** LDH release in *Nlr4*^{-/-} BMDMs infected with various *P. aeruginosa* strains
960 expressing or not *exoU* in presence of Ferrostatin-1 (Fe1, 10μM) for 2 hours.

961 **(B)** Measure of LDH release in various human and murine cell types infected with
962 various *P. aeruginosa* strains expressing or not *exoU* in presence of Ferrostatin-1
963 (Fe1, 10μM) for 2 hours.

964 **(C)** Immunoblotting of ExoU secretion by *P. aeruginosa* in presence of ferrostatin-1
965 (20μM).

966 **(D)** Measure of bacterial growth (O.D 600) in presence or absence of ferrostatin-1
967 (10, 20μM) for 14 hours)

968

969 **Figure S3: Lipid peroxidation fuels ExoU-dependent necrosis**

970 **(A)** ROS production in WT BMDMs transfected with ExoU or its catalytically dead
971 mutant ExoU^{S142A} for 45 minutes using H2DCFDA (1μM) probe.

972 **(B)** Lipidomic analysis of the relative amount of each phospholipid upon rExoU
973 transfection analysed in **Figure 3B**.

974 **(C)** Representative microscopy images of propidium iodide uptake in WT BMDMs
975 transfected with rExoU or its catalytically inactive mutant ExoU^{S142A} (500ng). Images
976 show two independent experiments, each performed three times at 45 minutes or 3
977 hours post transfection.

978 **(D)** Immunoblotting of Crispr Cas9-mediated *Gpx4* gene deletion in immortalized
979 BMDMs. The Gpx4#1 (red) was selected for further analysis. CD8 and GFP means
980 that cells were transduced with sgRNA targeting *Gfp* or *Cd8* genes and used as
981 controls.

982 **(E)** Cytometry detection and quantification of phospholipid peroxidation using the
983 probe C11-bodipy in immortalized WT or *Gpx4*^{-/-} BMDMs using a fortessa cytometer.

984 **(F)** PGE2 and LTB4 eicosanoid release in WT BMDMs transfected with 100ng of
985 ExoU or its catalytically dead mutant ExoU^{S142A} for 3 hours in presence or absence of
986 ferrostatin-1 (20μM).

987

988 **Figure S4: Ferrostatin-1 protects mice against ExoU-induced lung pathology**

989 **(A)** Gating strategy to analyse Immune cell populations in bronchoalveolar fluids
990 (BALFs). Immune cells were identified as CD45+ cells. Among CD45+ cells, different
991 subset of immune cells including Interstitial/Alveolar Macrophages, Eosinophils and
992 Neutrophils are identified based on specific cell surface marker expression.

993

994 **Graphical abstract: Host lipid peroxidation fuels ExoU-induced cell necrosis-**
995 **dependent pathology.** Upon injection into host target cells ExoU becomes hyper-
996 activated by host cell peroxidised phospholipids, which drives an exacerbated cell
997 necrosis and contributes to the subsequent pathology. Consequently, targeting lipid
998 peroxidation (ferrostatin-1) inhibits ExoU-dependent cell necrosis and attenuates the
999 host deleterious consequences.

1000

1001 **Movie S1: Live cell imaging of uninfected immortalized murine *Nlrc4*^{-/-} BMDMs**
1002 **cell death using SYTOX green. 1 “time point” corresponds to 150s.**

1003 **Movie S2: Live cell imaging of uninfected immortalized murine *Nlrc4*^{-/-} BMDMs**
1004 **cell death in presence of 20μM of ferrostatin-1 using SYTOX green. 1 “time**
1005 **point” corresponds to 150s.**

1006 **Movie S3: Live cell imaging of immortalized murine *Nlrc4*^{-/-} BMDMs cell death**
1007 **infected with *exoU*-expressing *P. aeruginosa* (MOI1) using SYTOX green. 1**
1008 **“time point” corresponds to 150s.**

1009 **Movie S4: Live cell imaging of immortalized murine *Nlrc4*^{-/-} BMDMs cell death**
1010 **infected with *exoU*-expressing *P. aeruginosa* (MOI1) in presence of ferrostatin-**
1011 **1 (20μM) using SYTOX green. 1 “time point” corresponds to 150s.**

1012 **Movie S5: Live cell imaging of immortalized murine *Nlrc4*^{-/-} BMDMs cell death**
1013 **infected with *exoU*-deficient *P. aeruginosa* (MOI1) using SYTOX green. 1 “time**
1014 **point” corresponds to 150s.**

1015 **Movie S6: Live cell imaging of immortalized murine *Nlrc4*^{-/-} BMDMs cell death**
1016 **infected with *exoU*-deficient *P. aeruginosa* (MOI1) in presence of ferrostatin-1**
1017 **(20μM) using SYTOX green. 1 “time point” corresponds to 150s.**

1018 **Movie S7: Live cell imaging of uninfected human bronchial organoids using**
1019 **Propidium Iodide up to 12 hours.**

1020 **Movie S8: Live cell imaging of uninfected human bronchial organoids in**
1021 **presence of ferrostatin-1 (40μM) using Propidium Iodide up to 12 hours.**

1022 **Movie S9: Live cell imaging of human bronchial organoids microinjected with**
1023 ***exoU*-expressing *P. aeruginosa* using Propidium Iodide up to 12 hours.**

1024 **Movie S10: Live cell imaging of human bronchial organoids microinjected with**
1025 ***exoU*-expressing *P. aeruginosa* in presence of ferrostatin-1 (40μM) using**
1026 **Propidium Iodide up to 12 hours.**

1027 **Movie S11: Live cell imaging of human bronchial organoids microinjected with**
1028 ***exoU*-deficient *P. aeruginosa* using Propidium Iodide up to 12 hours.**

1029 **Movie S12: Live cell imaging of human bronchial organoids microinjected with**
1030 ***exoU*-deficient *P. aeruginosa* in presence of ferrostatin-1 (40μM) using**
1031 **Propidium Iodide up to 12 hours.**

1032

1033

1034

1035

1036

1037

1038

1039

1040

1041

1042

1043

1044

1045

1046

1047

1048

1049

1050

1051

1052

1053

1054 **References**

1055 Amaral, E.P., Costa, D.L., Namasivayam, S., Riteau, N., Kamenyeva, O., Mittereder,
1056 L., Mayer-Barber, K.D., Andrade, B.B., and Sher, A. (2019). A major role for
1057 ferroptosis in *Mycobacterium tuberculosis*–induced cell death and tissue necrosis. *J.*
1058 *Exp. Med.* *216*, 556–570.

1059 Anderson, D.M., Sato, H., Dirck, A.T., Feix, J.B., and Frank, D.W. (2015). Ubiquitin
1060 activates patatin-like phospholipases from multiple bacterial species. *J. Bacteriol.*
1061 *197*, 529–541.

1062 Aoyagi, T., Newstead, M.W., Zeng, X., Nanjo, Y., Peters-Golden, M., Kaku, M., and
1063 Standiford, T.J. (2017). Interleukin-36 γ and IL-36 receptor signaling mediate impaired
1064 host immunity and lung injury in cytotoxic *Pseudomonas aeruginosa* pulmonary
1065 infection: Role of prostaglandin E2. *PLoS Pathog.* *13*.

1066 Balakrishnan, A., Karki, R., Berwin, B., Yamamoto, M., and Kanneganti, T.-D. (2018).

- 1067 Guanylate binding proteins facilitate caspase-11-dependent pyroptosis in response to
1068 type 3 secretion system-negative *Pseudomonas aeruginosa*. *Cell Death Discov.* **4**,
1069 66.
- 1070 Bartfeld, S., and Clevers, H. (2015). Organoids as model for infectious diseases:
1071 Culture of human and murine stomach organoids and microinjection of helicobacter
1072 pylori. *J. Vis. Exp.* **2015**.
- 1073 Beatty, A., Singh, T., Tyurina, Y.Y., Nicolas, E., Maslar, K., Zhou, Y., Cai, K.Q., Tan,
1074 Y., Doll, S., Conrad, M., et al. Conjugated linolenic fatty acids trigger ferroptosis in
1075 triple-negative breast cancer.
- 1076 Bedoui, S., Herold, M.J., and Strasser, A. (2020). Emerging connectivity of
1077 programmed cell death pathways and its physiological implications. *Nat. Rev. Mol.*
1078 *Cell Biol.* **21**, 678–695.
- 1079 Beharier, O., Tyurin, V.A., Goff, J.P., Guerrero-Santoro, J., Kajiwara, K., Chu, T.,
1080 Tyurina, Y.Y., St Croix, C.M., Wallace, C.T., Parry, S., et al. (2020). PLA2G6 guards
1081 placental trophoblasts against ferroptotic injury. *Proc. Natl. Acad. Sci. U. S. A.* **117**,
1082 27319–27328.
- 1083 Bersuker, K., Hendricks, J.M., Li, Z., Magtanong, L., Ford, B., Tang, P.H., Roberts,
1084 M.A., Tong, B., Maimone, T.J., Zoncu, R., et al. (2019). The CoQ oxidoreductase
1085 FSP1 acts parallel to GPX4 to inhibit ferroptosis. *Nature* **575**, 688–692.
- 1086 Bitto, N.J., Baker, P.J., Dowling, J.K., Wray-McCann, G., De Paoli, A., Tran, L.S.,
1087 Leung, P.L., Stacey, K.J., Mansell, A., Masters, S.L., et al. (2018). Membrane
1088 vesicles from *Pseudomonas aeruginosa* activate the noncanonical inflammasome
1089 through caspase-5 in human monocytes. *Immunol. Cell Biol.* **96**, 1120–1130.
- 1090 Bochkov, V.N., Oskolkova, O. V., Birukov, K.G., Levonen, A.L., Binder, C.J., and
1091 Stöckl, J. (2010). Generation and biological activities of oxidized phospholipids.
1092 *Antioxidants Redox Signal.* **12**, 1009–1059.
- 1093 Bogacz, M., and Krauth-Siegel, R.L. (2018). Tryparedoxin peroxidase-deficiency
1094 commits trypanosomes to ferroptosis-type cell death. *Elife* **7**.
- 1095 Cayrol, C., Duval, A., Schmitt, P., Roga, S., Camus, M., Stella, A., Burlet-Schiltz, O.,
1096 Gonzalez-De-Peredo, A., and Girard, J.P. (2018). Environmental allergens induce

- 1097 allergic inflammation through proteolytic maturation of IL-33. *Nat. Immunol.* *19*, 375–
1098 385.
- 1099 Cohen, T.S., and Prince, A.S. (2013). Activation of inflammasome signaling mediates
1100 pathology of acute *P. aeruginosa* pneumonia. *J. Clin. Invest.* *123*, 1630–1637.
- 1101 Conrad, M., and Pratt, D.A. (2019). The chemical basis of ferroptosis. *Nat. Chem.*
1102 *Biol.* *15*, 1137–1147.
- 1103 Conrad, M., Kagan, V.E., Bayir, H., Pagnussat, G.C., Head, B., Traber, M.G., and
1104 Stockwell, B.R. (2018). Regulation of lipid peroxidation and ferroptosis in diverse
1105 species. *Genes Dev.* *32*, 602–619.
- 1106 da Cunha, L.G., Ferreira, M.F., de Moraes, J.A., Reis, P.A., Castro-Faria-Neto, H.C.,
1107 Barja-Fidalgo, C., Plotkowski, M.C., and Saliba, A.M. (2015). ExoU-induced redox
1108 imbalance and oxidative stress in airway epithelial cells during *Pseudomonas*
1109 *aeruginosa* pneumosepsis. *Med. Microbiol. Immunol.* *204*, 673–680.
- 1110 Dar, H.H., Tyurina, Y.Y., Mikulska-Ruminska, K., Shrivastava, I., Ting, H.C., Tyurin,
1111 V.A., Krieger, J., Croix, C.M.S., Watkins, S., Bayir, E., et al. (2018). *Pseudomonas*
1112 *aeruginosa* utilizes host polyunsaturated phosphatidylethanolamines to trigger theft-
1113 ferroptosis in bronchial epithelium. *J. Clin. Invest.* *128*, 4639–4653.
- 1114 Demarco, B., Grayczyk, J.P., Bjanec, E., Roy, D. Le, Tonnus, W., Assenmacher,
1115 C.A., Radaelli, E., Fettlelet, T., Mack, V., Linkermann, A., et al. (2020). Caspase-8-
1116 dependent gasdermin D cleavage promotes antimicrobial defense but confers
1117 susceptibility to TNF-induced lethality. *Sci. Adv.* *6*, 3465–3483.
- 1118 Deruelle, V., Bouillot, S., Job, V., Taillebourg, E., Fauvarque, M.-O., Attrée, I., and
1119 Huber, P. (2020). The bacterial toxin ExoU requires a host trafficking chaperone for
1120 transportation and to induce necrosis. *BioRxiv* 2020.11.04.367706.
- 1121 Dessen, A. (2000). Phospholipase A2 enzymes: Structural diversity in lipid
1122 messenger metabolism. *Structure* *8*, R15–R22.
- 1123 Diaz, M.H., and Hauser, A.R. (2010). *Pseudomonas aeruginosa* cytotoxin ExoU is
1124 injected into phagocytic cells during acute pneumonia. *Infect. Immun.* *78*, 1447–
1125 1456.
- 1126 Dixon, S.J., Lemberg, K.M., Lamprecht, M.R., Skouta, R., Zaitsev, E.M., Gleason,

- 1127 C.E., Patel, D.N., Bauer, A.J., Cantley, A.M., Yang, W.S., et al. (2012). Ferroptosis:
1128 An iron-dependent form of nonapoptotic cell death. *Cell* 149, 1060–1072.
- 1129 Doll, S., Proneth, B., Tyurina, Y.Y., Panzilius, E., Kobayashi, S., Ingold, I., Irmeler, M.,
1130 Beckers, J., Aichler, M., Walch, A., et al. (2017). ACSL4 dictates ferroptosis
1131 sensitivity by shaping cellular lipid composition. *Nat. Chem. Biol.* 13, 91–98.
- 1132 Doll, S., Freitas, F.P., Shah, R., Aldrovandi, M., da Silva, M.C., Ingold, I., Grocin,
1133 A.G., Xavier da Silva, T.N., Panzilius, E., Scheel, C.H., et al. (2019). FSP1 is a
1134 glutathione-independent ferroptosis suppressor. *Nature* 575, 693–698.
- 1135 Dyer, K.D., Moser, J.M., Czapiga, M., Siegel, S.J., Percopo, C.M., and Rosenberg,
1136 H.F. (2008). Functionally Competent Eosinophils Differentiated Ex Vivo in High Purity
1137 from Normal Mouse Bone Marrow. *J. Immunol.* 181, 4004–4009.
- 1138 Eren, E., Planès, R., Buyck, J., Bordignon, P.-J., Colom, A., Cunrath, O., Dreier, R.,
1139 Santos, J., Duplan-Eche, V., Näser, E., et al. (2019). Type-3 Secretion System–
1140 induced pyroptosis protects *Pseudomonas* against cell-autonomous immunity.
1141 *BioRxiv* 650333.
- 1142 Eren, E., Planès, R., Bagayoko, S., Bordignon, P., Chaoui, K., Hessel, A., Santoni,
1143 K., Pinilla, M., Lagrange, B., Bulet-Schiltz, O., et al. (2020). *Irgm2* and *Gate-16*
1144 cooperatively dampen Gram-negative bacteria-induced caspase-11 response. *EMBO*
1145 *Rep.* 21.
- 1146 Faure, E., Mear, J.B., Faure, K., Normand, S., Couturier-Maillard, A., Grandjean, T.,
1147 Balloy, V., Ryffel, B., Dessein, R., Chignard, M., et al. (2014). *Pseudomonas*
1148 *aeruginosa* type-3 secretion system dampens host defense by exploiting the NLRC4-
1149 coupled inflammasome. *Am. J. Respir. Crit. Care Med.* 189, 799–811.
- 1150 Flores-Díaz, M., Monturiol-Gross, L., Naylor, C., Alape-Girón, A., and Flieger, A.
1151 (2016). Bacterial Sphingomyelinases and Phospholipases as Virulence Factors.
1152 *Microbiol. Mol. Biol. Rev.* 80, 597–628.
- 1153 Franchi, L., Stoolman, J., Kanneganti, T.D., Verma, A., Ramphal, R., and Núñez, G.
1154 (2007). Critical role for *Ipaf* in *Pseudomonas aeruginosa*-induced caspase-1
1155 activation. *Eur. J. Immunol.* 37, 3030–3039.
- 1156 Friedmann Angeli, J.P., Schneider, M., Proneth, B., Tyurina, Y.Y., Tyurin, V.A.,

- 1157 Hammond, V.J., Herbach, N., Aichler, M., Walch, A., Eggenhofer, E., et al. (2014).
1158 Inactivation of the ferroptosis regulator Gpx4 triggers acute renal failure in mice. *Nat.*
1159 *Cell Biol.* *16*, 1180–1191.
- 1160 Galluzzi, L., Vitale, I., Aaronson, S.A., Abrams, J.M., Adam, D., Agostinis, P.,
1161 Alnemri, E.S., Altucci, L., Amelio, I., Andrews, D.W., et al. (2018). Molecular
1162 mechanisms of cell death: Recommendations of the Nomenclature Committee on
1163 Cell Death 2018. *Cell Death Differ.* *25*, 486–541.
- 1164 Gendrin, C., Contreras-Martel, C., Bouillot, S., Elsen, S., Lemaire, D., Skoufias, D.A.,
1165 Huber, P., Attree, I., and Dessen, A. (2012). Structural Basis of Cytotoxicity Mediated
1166 by the Type III Secretion Toxin ExoU from *Pseudomonas aeruginosa*. *PLoS Pathog.*
1167 *8*, e1002637.
- 1168 Hiu, J.J., and Yap, M.K.K. (2020). Cytotoxicity of snake venom enzymatic toxins:
1169 Phospholipase A2 and L-amino acid oxidase. *Biochem. Soc. Trans.* *48*, 719–731.
- 1170 Howell, H.A., Logan, L.K., and Hauser, A.R. (2013). Type III secretion of ExoU is
1171 critical during early *Pseudomonas aeruginosa* Pneumonia. *MBio* *4*.
- 1172 Iannitti, R.G., Napolioni, V., Oikonomou, V., De Luca, A., Galosi, C., Pariano, M.,
1173 Massi-Benedetti, C., Borghi, M., Puccetti, M., Lucidi, V., et al. (2016). IL-1 receptor
1174 antagonist ameliorates inflammasome-dependent inflammation in murine and human
1175 cystic fibrosis. *Nat. Commun.* *7*, 1–16.
- 1176 Jenkins, N.L., James, S.A., Salim, A., Sumardy, F., Speed, T.P., Conrad, M.,
1177 Richardson, D.R., Bush, A.I., and McColl, G. (2020). Changes in ferrous iron and
1178 glutathione promote ferroptosis and frailty in aging *Caenorhabditis elegans*. *Elife* *9*, 1–
1179 28.
- 1180 Kagan, V.E., Mao, G., Qu, F., Angeli, J.P.F., Doll, S., Croix, C.S., Dar, H.H., Liu, B.,
1181 Tyurin, V.A., Ritov, V.B., et al. (2017). Oxidized arachidonic and adrenic PEs
1182 navigate cells to ferroptosis. *Nat. Chem. Biol.* *13*, 81–90.
- 1183 Kain, H.S., Glennon, E.K.K., Vijayan, K., Arang, N., Douglass, A.N., Fortin, C.L.,
1184 Zuck, M., Lewis, A.J., Whiteside, S.L., Dudgeon, D.R., et al. (2020). Liver stage
1185 malaria infection is controlled by host regulators of lipid peroxidation. *Cell Death*
1186 *Differ.* *27*, 44–54.

- 1187 Kinsey, G.R., Blum, J.L., Covington, M.D., Cummings, B.S., McHowat, J., and
1188 Schnellmann, R.G. (2008). Decreased iPLA2 γ expression induces lipid peroxidation
1189 and cell death and sensitizes cells to oxidant-induced apoptosis. *J. Lipid Res.* *49*,
1190 1477–1487.
- 1191 van Kuijk, F.J.G.M., Sevanian, A., Handelman, G.J., and Dratz, E.A. (1987). A new
1192 role for phospholipase A2: protection of membranes from lipid peroxidation damage.
1193 *Trends Biochem. Sci.* *12*, 31–34.
- 1194 Lefèvre, L., Authier, H., Stein, S., Majorel, C., Couderc, B., Dardenne, C., Eddine,
1195 M.A., Meunier, E., Bernad, J., Valentin, A., et al. (2015). LRH-1 mediates anti-
1196 inflammatory and antifungal phenotype of IL-13-activated macrophages through the
1197 PPAR γ ligand synthesis. *Nat. Commun.* *6*, 1–13.
- 1198 Li, N., Wang, W., Zhou, H., Wu, Q., Duan, M., Liu, C., Wu, H., Deng, W., Shen, D.,
1199 and Tang, Q. (2020). Ferritinophagy-mediated ferroptosis is involved in sepsis-
1200 induced cardiac injury. *Free Radic. Biol. Med.* *160*, 303–318.
- 1201 Li, P., Allen, H., Banerjee, S., Franklin, S., Herzog, L., Johnston, C., McDowell, J.,
1202 Paskind, M., Rodman, L., Salfeld, J., et al. (1995). Mice deficient in IL-1 β -converting
1203 enzyme are defective in production of mature IL-1 β and resistant to endotoxic shock.
1204 *Cell* *80*, 401–411.
- 1205 Lovatt, M., Adnan, K., Kocaba, V., Dirisamer, M., Peh, G.S.L., and Mehta, J.S.
1206 (2020). Peroxiredoxin-1 regulates lipid peroxidation in corneal endothelial cells.
1207 *Redox Biol.* *30*, 101417.
- 1208 Lu, B., Chen, X. bing, Hong, Y. cai, Zhu, H., He, Q. jun, Yang, B., Ying, M. dan, and
1209 Cao, J. (2019). Identification of PRDX6 as a regulator of ferroptosis. *Acta Pharmacol.*
1210 *Sin.* *40*, 1334–1342.
- 1211 Machado, G.B., de Oliveira, A. V., Saliba, A.M., de Lima, C.D.M., Suassuna, J.H.R.,
1212 and Plotkowski, M.C. (2011). *Pseudomonas aeruginosa* toxin ExoU induces a PAF-
1213 dependent impairment of alveolar fibrin turnover secondary to enhanced activation of
1214 coagulation and increased expression of plasminogen activator inhibitor-1 in the
1215 course of mice pneumosepsis. *Respir. Res.* *12*, 104.
- 1216 Man, S.M., Hopkins, L.J., Nugent, E., Cox, S., Glück, I.M., Turlomousis, P., Wright,
1217 J.A., Cicuta, P., Monie, T.P., and Bryant, C.E. (2014). Inflammasome activation

- 1218 causes dual recruitment of NLRC4 and NLRP3 to the same macromolecular
1219 complex. *Proc. Natl. Acad. Sci. U. S. A.* *111*, 7403–7408.
- 1220 Meunier, E., and Neyrolles, O. (2019). Die another way: Ferroptosis drives
1221 tuberculosis pathology. *J. Exp. Med.* *216*, 471–473.
- 1222 Miao, E.A., Ernst, R.K., Dors, M., Mao, D.P., and Aderem, A. (2008). *Pseudomonas*
1223 *aeruginosa* activates caspase 1 through Ipaf. *Proc. Natl. Acad. Sci. U. S. A.* *105*,
1224 2562–2567.
- 1225 Miyamoto, S., Dupas, C., Murota, K., and Terao, J. (2003). Phospholipid
1226 hydroperoxides are detoxified by phospholipase A2 and GSH peroxidase in rat
1227 gastric mucosa. *Lipids* *38*, 641–649.
- 1228 Al Moussawi, K., and Kazmierczak, B.I. (2014). Distinct contributions of interleukin-1 α
1229 (IL-1 α) and IL-1 β to innate immune recognition of *Pseudomonas aeruginosa* in the
1230 lung. *Infect. Immun.* *82*, 4204–4211.
- 1231 Palm, N.W., Rosenstein, R.K., Yu, S., Schenten, D.D., Florsheim, E., and Medzhitov,
1232 R. (2013). Bee venom phospholipase A2 induces a primary type 2 response that is
1233 dependent on the receptor ST2 and confers protective immunity. *Immunity* *39*, 976–
1234 985.
- 1235 Pazos, M.A., Lanter, B.B., Yonker, L.M., Eaton, A.D., Pirzai, W., Gronert, K.,
1236 Bonventre, J. V., and Hurley, B.P. (2017). *Pseudomonas aeruginosa* ExoU augments
1237 neutrophil transepithelial migration. *PLoS Pathog.* *13*.
- 1238 Phillips, R.M., Six, D.A., Dennis, E.A., and Ghosh, P. (2003). In Vivo Phospholipase
1239 Activity of the *Pseudomonas aeruginosa* Cytotoxin ExoU and Protection of
1240 Mammalian Cells with Phospholipase A2 Inhibitors. *J. Biol. Chem.* *278*, 41326–
1241 41332.
- 1242 Place, D.E., Lee, S.J., and Kanneganti, T.D. (2021). PANoptosis in microbial
1243 infection. *Curr. Opin. Microbiol.* *59*, 42–49.
- 1244 Rabin, S.D.P., and Hauser, A.R. (2003). *Pseudomonas aeruginosa* ExoU, a toxin
1245 transported by the type III secretion system, kills *Saccharomyces cerevisiae*. *Infect.*
1246 *Immun.* *71*, 4144–4150.
- 1247 Sachs, N., Papaspyropoulos, A., Zomer-van Ommen, D.D., Heo, I., Böttinger, L.,

- 1248 Klay, D., Weeber, F., Huelsz-Prince, G., Iakobachvili, N., Amatngalim, G.D., et al.
1249 (2019). Long-term expanding human airway organoids for disease modeling. *EMBO*
1250 *J.* **38**.
- 1251 Sadikot, R.T., Zeng, H., Azim, A.C., Joo, M., Dey, S.K., Beyer, R.M., Pebbles, R.S.,
1252 Blackwell, T.S., and Christman, J.W. (2007). Bacterial clearance of *Pseudomonas*
1253 *aeruginosa* is enhanced by the inhibition of COX-2. *Eur. J. Immunol.* **37**, 1001–1009.
- 1254 Saliba, A.M., Nascimento, D.O., Silva, M.C.A., Assis, M.C., Gayer, C.R.M.,
1255 Raymond, B., Coelho, M.G.P., Marques, E.A., Touqui, L., Albano, R.M., et al. (2005).
1256 Eicosanoid-mediated proinflammatory activity of *pseudomonas aeruginosa* ExoU.
1257 *Cell. Microbiol.* **7**, 1811–1822.
- 1258 Saliba, A.M., De Assis, M.C., Nishi, R., Raymond, B., Marques, E.D.A., Lopes, U.G.,
1259 Touqui, L., and Plotkowski, M.C. (2006). Implications of oxidative stress in the
1260 cytotoxicity of *Pseudomonas aeruginosa* ExoU. *Microbes Infect.* **8**, 450–459.
- 1261 Santos, J.C., Dick, M.S., Lagrange, B., Degrandi, D., Pfeffer, K., Yamamoto, M.,
1262 Meunier, E., Pelczar, P., Henry, T., and Broz, P. (2018). <scp>LPS</scp> targets
1263 host guanylate-binding proteins to the bacterial outer membrane for non-canonical
1264 inflammasome activation. *EMBO J.* **37**.
- 1265 Sato, H., and Frank, D.W. (2004). ExoU is a potent intracellular phospholipase. *Mol.*
1266 *Microbiol.* **53**, 1279–1290.
- 1267 Sevanian, A., Wratten, M. Lou, McLeod, L.L., and Kim, E. (1988). Lipid peroxidation
1268 and phospholipase A2 activity in liposomes composed of unsaturated phospholipids:
1269 a structural basis for enzyme activation. *Biochim. Biophys. Acta (BBA)/Lipids Lipid*
1270 *Metab.* **961**, 316–327.
- 1271 Shaver, C.M., and Hauser, A.R. (2004). Relative contributions of *Pseudomonas*
1272 *aeruginosa* ExoU, ExoS, and ExoT to virulence in the lung. *Infect. Immun.* **72**, 6969–
1273 6977.
- 1274 Sitkiewicz, I., Nagiec, M.J., Sumbly, P., Butler, S.D., Cywes-Bentley, C., and Musser,
1275 J.M. (2006). Emergence of a bacterial clone with enhanced virulence by acquisition
1276 of a phage encoding a secreted phospholipase A2. *Proc. Natl. Acad. Sci. U. S. A.*
1277 **103**, 16009–16014.

- 1278 Sitkiewicz, I., Stockbauer, K.E., and Musser, J.M. (2007). Secreted bacterial
1279 phospholipase A2 enzymes: better living through phospholipolysis. *Trends Microbiol.*
1280 *15*, 63–69.
- 1281 Skouta, R., Dixon, S.J., Wang, J., Dunn, D.E., Orman, M., Shimada, K., Rosenberg,
1282 P.A., Lo, D.C., Weinberg, J.M., Linkermann, A., et al. (2014). Ferrostatis inhibit
1283 oxidative lipid damage and cell death in diverse disease models. *J. Am. Chem. Soc.*
1284 *136*, 4551–4556.
- 1285 Stockwell, B.R., Jiang, X., and Gu, W. (2020). Emerging Mechanisms and Disease
1286 Relevance of Ferroptosis.
- 1287 Sutterwala, F.S., Mijares, L.A., Li, L., Ogura, Y., Kazmierczak, B.I., and Flavell, R.A.
1288 (2007). Immune recognition of *Pseudomonas aeruginosa* mediated by the
1289 IPAF/NLRC4 inflammasome. *J. Exp. Med.* *204*, 3235–3245.
- 1290 Tamura, M., Ajayi, T., Allmond, L.R., Moriyama, K., Wiener-Kronish, J.P., and Sawa,
1291 T. (2004). Lysophospholipase A activity of *Pseudomonas aeruginosa* type III
1292 secretory toxin ExoU. *Biochem. Biophys. Res. Commun.* *316*, 323–331.
- 1293 Tang, L., Lu, C., Zheng, G., and Burgering, B.M.T. (2020). Emerging insights on the
1294 role of gasdermins in infection and inflammatory diseases. *Clin. Transl. Immunol.* *9*.
- 1295 Troegeler, A., Lastrucci, C., Duval, C., Tanne, A., Cougoule, C., Maridonneau-Parini,
1296 I., Neyrolles, O., and Lugo-Villarino, G. (2014). An efficient siRNA-mediated gene
1297 silencing in primary human monocytes, dendritic cells and macrophages. *Immunol.*
1298 *Cell Biol.* *92*, 699–708.
- 1299 Tyurin, V.A., Balasubramanian, K., Winnica, D., Tyurina, Y.Y., Vikulina, A.S., He,
1300 R.R., Kapralov, A.A., Macphee, C.H., and Kagan, V.E. (2014). Oxidatively modified
1301 phosphatidylserines on the surface of apoptotic cells are essential phagocytic “eat-
1302 me” signals: Cleavage and inhibition of phagocytosis by Lp-PLA 2. *Cell Death Differ.*
1303 *21*, 825–835.
- 1304 Tyurina, Y.Y., Tyurin, V.A., Anthony-muthu, T., Amoscato, A.A., Sparvero, L.J.,
1305 Nesterova, A.M., Baynard, M.L., Sun, W., He, R.R., Khaitovich, P., et al. (2019).
1306 “Redox lipidomics technology: Looking for a needle in a haystack.” *Chem. Phys.*
1307 *Lipids* *221*, 93–107.

- 1308 Wiernicki, B., Dubois, H., Tyurina, Y.Y., Hassannia, B., Bayir, H., Kagan, V.E.,
1309 Vandenabeele, P., Wullaert, A., and Vanden Berghe, T. (2020). Excessive
1310 phospholipid peroxidation distinguishes ferroptosis from other cell death modes
1311 including pyroptosis. *Cell Death Dis.* *11*, 922.
- 1312 Wilson, S.K., and Knoll, L.J. (2018). Patatin-like phospholipases in microbial
1313 infections with emerging roles in fatty acid metabolism and immune regulation by
1314 Apicomplexa. *Mol. Microbiol.* *107*, 34–46.
- 1315 Yan1, B., Ai1, Y., Zhang1, Z., Sun1, Q., Ma1, Y., Zhang1, Z., and Wang1, X. (2020).
1316 Oxidoreductases generate hydrogen peroxide that drives iron-dependent lipid
1317 peroxidation during ferroptosis 2 The inhibition of antioxidant systems of glutathione
1318 peroxidase 4 (GPX4) or ferroptosis suppressor protein 1 (FSP1) causes iron-
1319 dependent peroxid. *BioRxiv* 2020.08.01.231993.
- 1320 Yang, D., Han, Z., and Oppenheim, J.J. (2017). Alarmins and immunity. *Immunol.*
1321 *Rev.* *280*, 41–56.
- 1322 Yang, W.S., Kim, K.J., Gaschler, M.M., Patel, M., Shchepinov, M.S., and Stockwell,
1323 B.R. (2016). Peroxidation of polyunsaturated fatty acids by lipoxygenases drives
1324 ferroptosis. *Proc. Natl. Acad. Sci. U. S. A.* *113*, E4966–E4975.
- 1325 Yedgar, S., Cohen, Y., and Shoseyov, D. (2006). Control of phospholipase A2
1326 activities for the treatment of inflammatory conditions. *Biochim. Biophys. Acta - Mol.*
1327 *Cell Biol. Lipids* *1761*, 1373–1382.
- 1328 Zhu, H., Santo, A., Jia, Z., and Li, Y. (2019). GPx4 in Bacterial Infection and
1329 Polymicrobial Sepsis: Involvement of Ferroptosis and Pyroptosis. *React. Oxyg.*
1330 *Species* *7*, 154.
- 1331 Zou, Y., Li, H., Graham, E.T., Deik, A.A., Eaton, J.K., Wang, W., Sandoval-Gomez,
1332 G., Clish, C.B., Doench, J.G., and Schreiber, S.L. (2020). Cytochrome P450
1333 oxidoreductase contributes to phospholipid peroxidation in ferroptosis. *Nat. Chem.*
1334 *Biol.* *16*, 302–309.
- 1335
- 1336
- 1337

1338

1339

1340

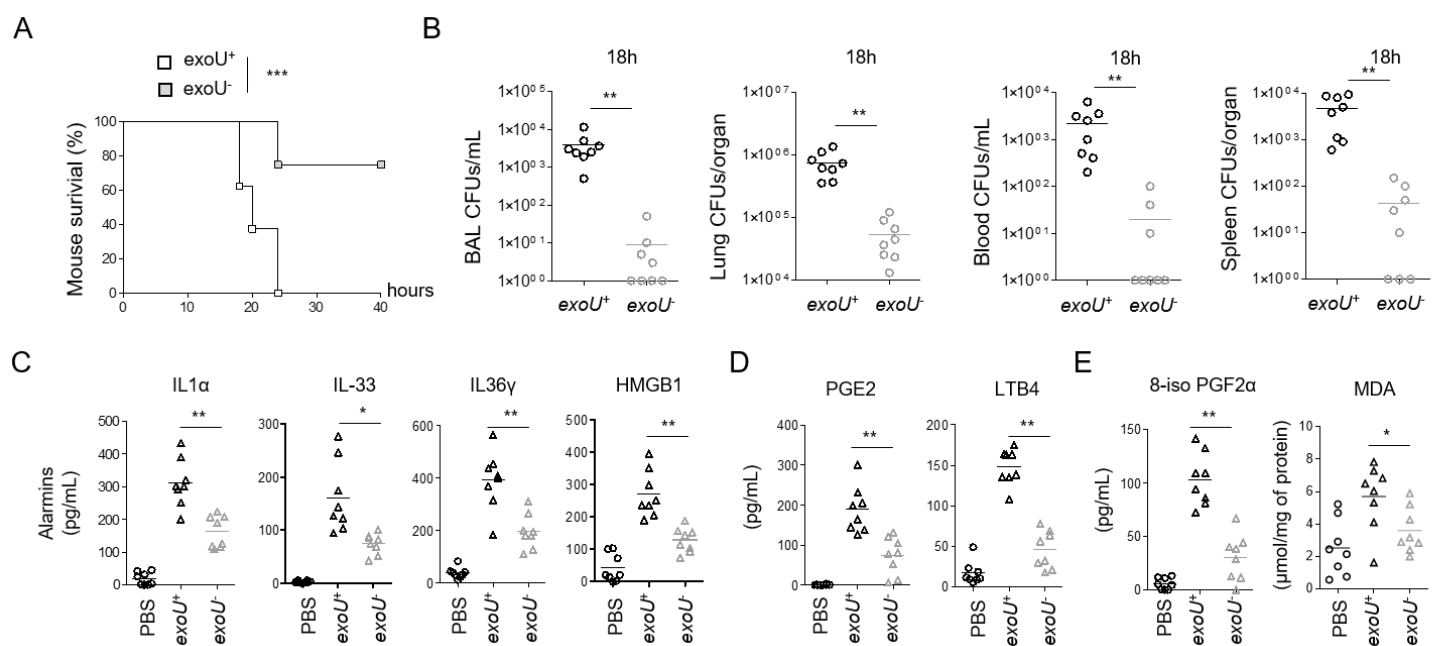
1341

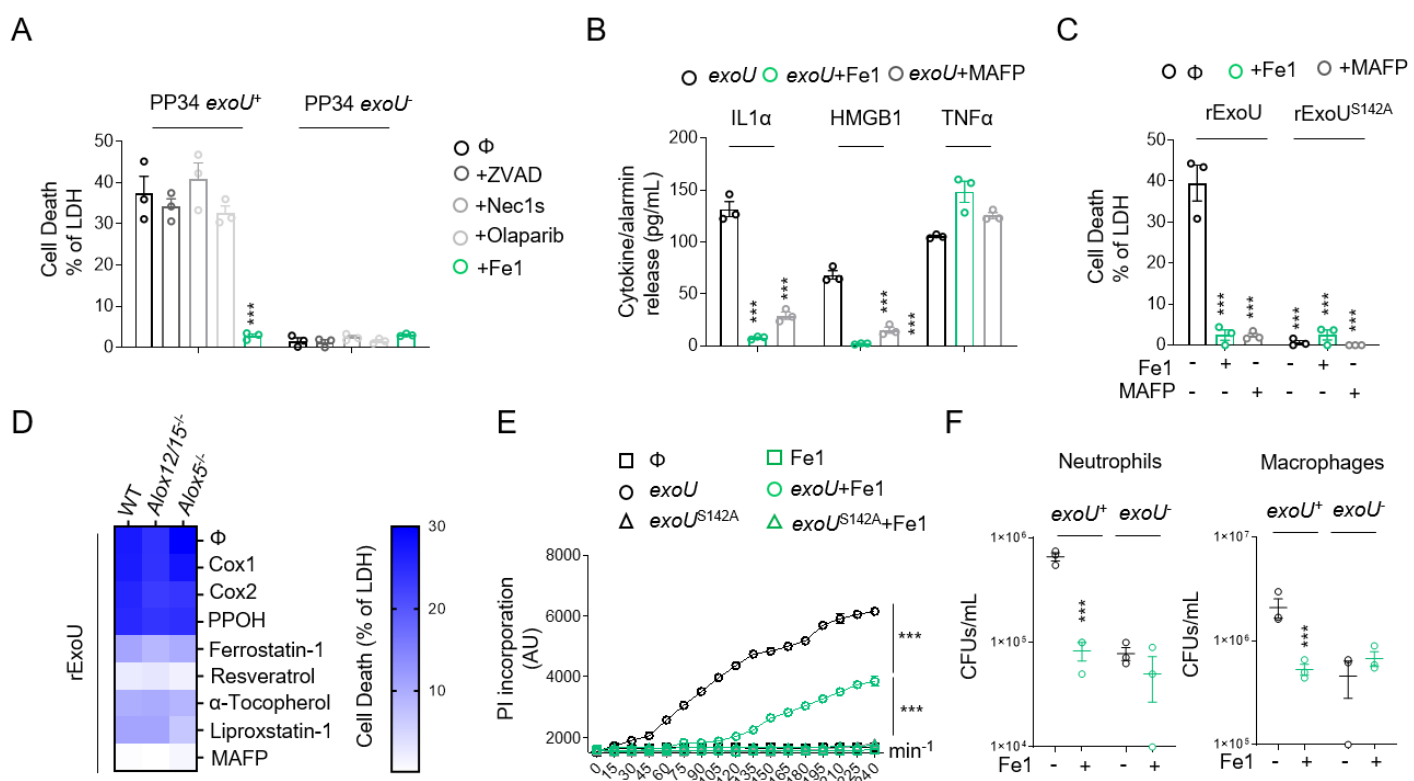
1342

1343

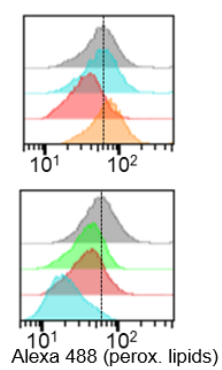
1344

1345

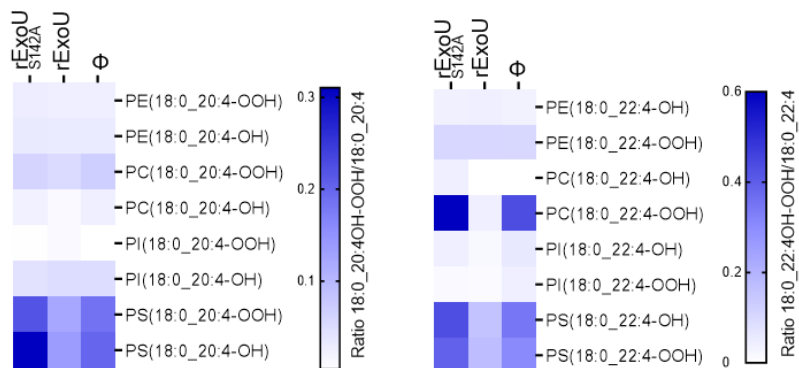




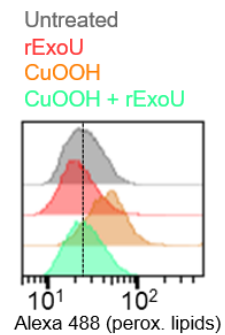
A



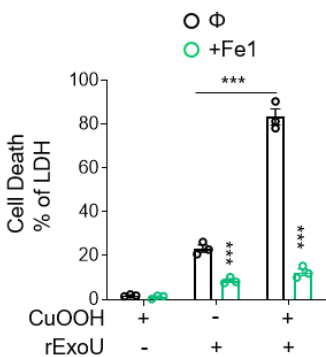
B



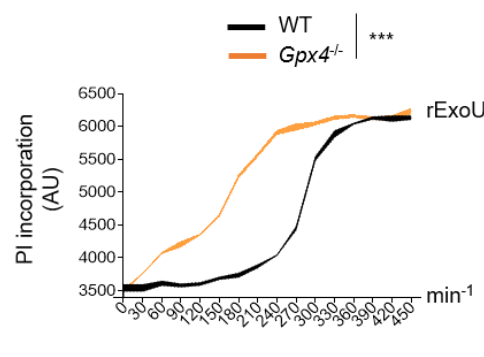
C



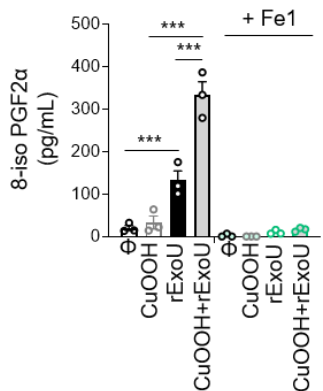
D



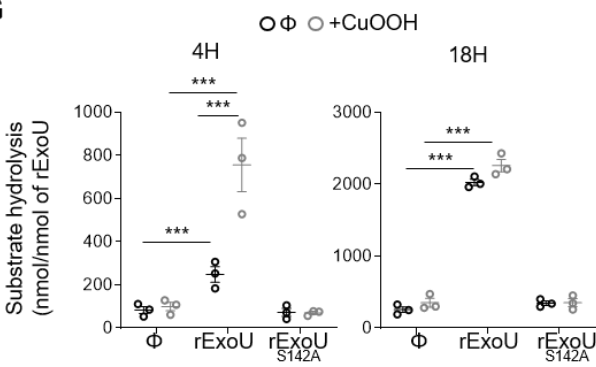
E



F



G



H

